J|A|C|S ARTICLES

Published on Web 03/30/2009

Design, Synthesis, and Characterization of Ladder-Type Molecules and Polymers. Air-Stable, Solution-Processable *n*-Channel and Ambipolar Semiconductors for Thin-Film Transistors via Experiment and Theory

Hakan Usta, Chad Risko, Zhiming Wang, Hui Huang, Murat K. Deliomeroglu, Aleksandr Zhukhovitskiy, Antonio Facchetti,* and Tobin J. Marks*

Department of Chemistry and the Materials Research Center, Northwestern University, 2145 Sheridan Road, Evanston, Illinois, 60208

Received December 7, 2008; E-mail: a-facchetti@northwestern.edu (A.F.); t-marks@northwestern.edu (T.J.M.)

Abstract: The design, synthesis, and characterization of new high-performance n-channel molecular/polymeric semiconductors that are solution-processable and air-stable is of great interest for the development of p−n junctions, bipolar transistors, and organic complementary circuitry (CMOS). While over the past two decades there have been many reports on n-channel materials, solution-processability and air-stability still remain as major challenges. We report here the synthesis and detailed characterization of a highly electron-deficient class of indeno[1,2-b]fluorene-6,12-dione, 2,2′-(indeno[1,2-b]fluorene-6,12-diylidene) dimalononitrile, bisindenofluorene-12,15-dione, and 2,2′-(bisindenofluorene-12,15-diylidene) dimalononitrile-based ladder-type building blocks (**1**−**12**) and their corresponding homo- and copolymers (**P1**−**P14**), and examine in detail the effects of core size, thiophene vs core regiochemistry, carbonyl vs dicyanovinylene functionality, and alkyl chain orientation on the physicochemical properties, thin film microstructures, and OFET device performance. New compounds are characterized by DSC, TGA, melting point, single-crystal X-ray diffraction (XRD), solution/thin film optical, PL, and cyclic voltammetry measurements to evaluate frontier molecular orbital energetics and intermolecular cohesive forces. Thin films are grown by vacuum deposition and spin-coating, and investigated by X-ray diffraction (XRD) and AFM. By tuning the HOMO/LUMO energetics of the present materials over a 1.1 eV range, p-type, n-type, or ambipolar charge transport characteristics can be observed, thus identifying the MO energetic windows governing majority carrier polarity and air stability. One of these systems, thiophene-terminated indenofluorenedicyanovinylene **10** exhibits an electron mobility of 0.16 $cm^2/V \cdot s$ and an I_{on}/I_{off} ratio of 10^7-10^8, one of the highest to date for a solution-cast air-stable n-channel semiconductor. Here we also report solution-processed ambipolar films of thiophene-based molecule **12** and copolymers **P13** and **P14** which exhibit electron and hole mobilities of $1 \times 10^{-3}-2 \times 10^{-4}$ and I_{on}/I_{off} ratios of $\sim 10^4$, representing the first examples of molecular and polymeric ambipolar semiconductors to function in air. Analysis of the operational air-stabilities of a series of thin films having different crystallinities, orientations, and morphologies suggests that operational air-stability for thermodynamically predicted (i.e., no kinetic barrier contribution) air-stable semiconductors is principally governed by LUMO energetics with minimal contribution from thin-film microstructure. The onset LUMO energy for carrier electron stabilization is estimated as −4.0 to −4.1 eV, indicating an overpotential of 0.9−1.0 eV. Density functional theory calculations provide detailed insight into molecule/polymer physicochemical and charge transport characteristics.

Introduction

Over the past two decades, many classes of π-conjugated organic molecules and polymers have been synthesized and characterized as semiconductors for organic field-effect transistors (OFETs), mainly focusing on oligoacene and oligothiophene derivatives.[1,2] Due to the relatively air-stable hole-transporting characteristics of these cores and HOMO energies of ~ -4.9 to -5.5 eV, which aligns with the work function of air-stable electrodes (Au, 5.1 eV; Pt, 5.6 eV), most of these initial semiconductor examples were p-channel materials.[3] After the first report of n-channel OFETs based on metallophthalocyanines in 1990,[4] intensive research on the rational design and synthesis of new materials with high electron affinities has afforded several series of n-channel semiconductors in which electron-deficient substituents/units such as perfluoralkyl ($-C_nF_{2n+1}$), −CN, −F, perfluorophenyl (C_6F_5-), carbonyl (−C═O), and imide [−C(O)NHC(O)−] are incorporated into thiophene-, phenylene-, and arylene-based π-conjugated cores.[1,5] For these

(1) Facchetti, A. *Mater. Today* **2007**, *10*, 28–37.
(2) Murphy, A. R.; Frechet, J. M. J. *Chem. Rev.* **2007**, *107*, 1066–1096.
(3) Fichou, D. *Handbook of Oligo- and Polythiophenes*; Wiley-VCH, New York, 1998.
(4) Guillaud, G.; Sadound, M. Al; Maitrot, M *Chem. Phys. Lett.* **1990**, *167*, 503–506.

10.1021/ja809555c CCC: $40.75

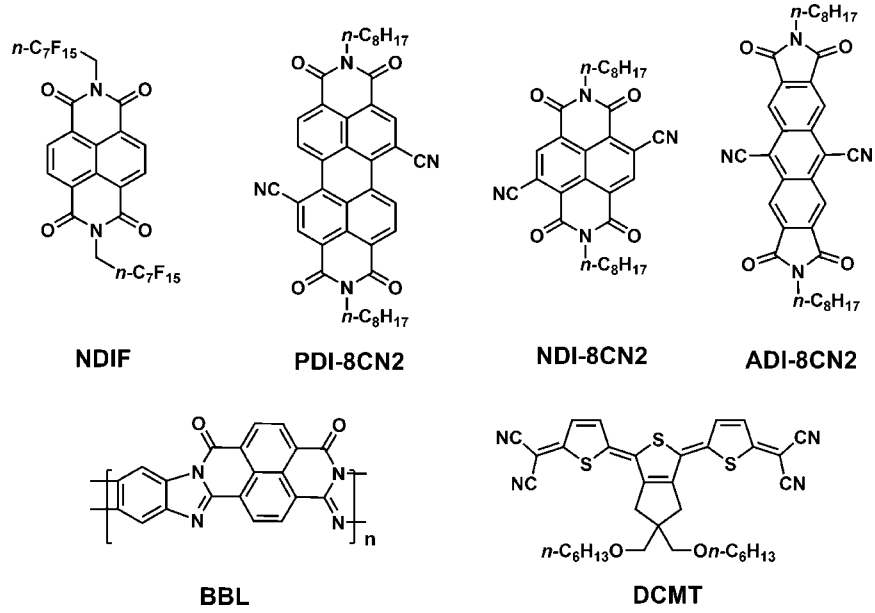

Figure 1. Structures of air-stable n-channel semiconductors.

semiconductors, electron mobilites as high as 0.1−2.0 $cm^2/V \cdot s$ are obtained under vacuum/nitrogen.[1] However, only a few of the current n-channel semiconductors exhibit air-stable FET device operation, and this is generally achieved via fluoroalkyl-based kinetic barriers and/or stabilization-imparting MO energetics,[6] with the exact mechanism of ambient stability not fully established.[7] Furthermore, while single-component ambipolar semiconductors were first reported in 2003,[8] only recently was an ambipolar coordination compound reported to operate in air with modest FET performance ($\mu_{e,h} = 10^{-4}$ $cm^2/V \cdot s$).[9] Thus, while today there are a number of n-channel materials and a few ambipolar materials having field-effect mobilities ≥ 0.1 $cm^2/V \cdot s$, two major challenges remain: (i) stabilizing the electrons during FET operation in ambient without device encapsulation and (ii) solution-processibility to eliminate costly vacuum/inert atmosphere-based deposition processes. To truly realize n-channel and ambipolar semiconductors in p−n junctions, bipolar transistors, and organic complementary circuitry (CMOS), additional device encapsulation should be avoided by enhancing ambient stability, and solubility should be increased to enable straightforward, solution-based deposition techniques such as spin-coating, drop-casting, and printing. Furthermore, the science governing device environmental stability and performance-processing relationships should be understood in greater depth.

To a first approximation, the ambient stability of n-channel semiconductors is controlled by the ionization potential of the injected/induced electrons, formed when the FET is in the accumulation regime, or in Koopmans' theorem[10] metrics, by the LUMO energy of the neutral semiconductor.[11] In general, lowering organic semiconductor LUMO energies enhances FET device stability by energetically stabilizing the induced electrons during charge transport, which occurs primarily by hopping through low-lying LUMOs.[6] The issue of ambient stability was initially addressed by de Leeuw et al. in 1997, focusing mainly on n-doped organic polymers which are rare compared to their p-doped counterparts.[11] Degradation of such materials in ambient is mainly due to reaction of the charge-carrying electrons with O_2 and H_2O, and is not related to intrinsic chemical instability. This process is also known as *trapping* and reduces the current flow through the FET conduction channel. Although the same trapping can be achieved by hydroxyl groups at the dielectric−semiconductor interface, the density of these trapping sites can be substantially reduced by hexamethyldisilazene (HMDS) or octadecyltrichlorosilane (OTS) surface treatments and is not relevant to the present discussion.

In one approach to realizing air-stable n-channel device operation, Katz et al. employed molecular semiconductors with perfluoroalkyl ($-C_nF_{2n+1}$) side chains (NDIF, Figure 1) which pack in a sufficiently dense thin-film motif to form a kinetic barrier against ambient species penetration.[12] A similar effect was also observed with perfluorinated copper phthalocyanine ($CuF_{16}Pc$) and fluorocarbon-substituted oligothiophenes (DFCO-4TCO).[13,14] Although these semiconductors exhibit initial ambient operational stability, depending on the O_2 partial pressure and film growth methodology, OFET performance degrades over periods of hours to days.[7] Hence, semiconductors exhibiting intrinsically (i.e., thermodynamically) air-stable electron transport not affected by enviromental conditions and film microstructure would be highly desirable.

As an initial approach, using solution-phase standard electrochemical potentials (eqs 1 and 2) and assuming pH 7.0 and

(5) Dimitrakopoulos, C. D.; Malenfant, P. R. L. *Adv. Mater.* **2002**, *14*, 99–117.
(6) Newman, C. R.; Frisbie, C. D.; Filho, D. A; da, S.; Brédas, J.-L.; Ewbank, P. C.; Mann, K. R *Chem. Mater.* **2004**, *16*, 4436–4451.
(7) Weitz, R. T.; Amsharov, K.; Zschieschang, U.; Villas, E. B.; Goswami, D. K.; Burghard, M.; Dosch, H.; Jansen, M.; Kern, K.; Klauk, H. *J. Am. Chem. Soc.* **2008**, *130*, 4637–4645.
(8) Meijer, E. J.; de Leeuw, D. M.; Setayesh, S.; van Veenendaal, E.; Huisman, B. H.; Blom, P. W. M.; Hummelen, J. C.; Scherf, U.; Klapwijk, T. M. *Nat. Mater.* **2003**, *2*, 678–682.
(9) Anthopoulos, T. D.; Setayesh, S.; Smits, E.; Coelle, M.; Cantatore, E.; Blom, P. W. M.; de Leeuw, D. M. *Adv. Mater.* **2006**, *18*, 1900–1904.
(10) Koopmans, T. *Physica* **1933**, *1*, 104.
(11) de Leeuw, D. M.; Simenon, M. M. J.; Brown, A. R.; Einerhand, R. E. F. *Synth. Met.* **1997**, *87*, 53–59.
(12) Katz, H. E.; Lovinger, A. J.; Johnson, J.; Kloc, C.; Seigrist, T.; Li, W.; Lin, Y.-Y.; Dodabalapur, A. *Nature* **2000**, *404*, 478–481.
(13) Yoon, M. H.; DiBenedetto, S. A.; Russell, M. T.; Facchetti, A.; Marks, T. J. *Chem. Mater.* **2007**, *19*, 4864–4881.
(14) Bao, Z.; Lovinger, A. J.; Brown, J. *J. Am. Chem. Soc.* **1998**, *120*, 207–208.

an overpotential of 0.0 V, the limits of the semiconductor reduction potentials for stability are estimated as ≥ −0.658 V (vs SCE) with respect to *H_2O oxidation*, and ≥ +0.571 V (vs SCE) with respect to *O_2 oxidation*.[11]

$$4e^- + 4H^+ + O_2 \rightarrow 2H_2O \quad E^\circ = +0.571 \text{ V (vs SCE)} \tag{1}$$

$$2e^- + 2H_2O \rightarrow H_2 + 2OH^- \quad E^\circ = -0.658 \text{ V (vs SCE)} \tag{2}$$

Although there are a number of π-conjugated organic materials having a first reduction potential greater than −0.658 V, electron-deficient molecules with reduction potentials surpassing +0.571 V are very rare. Thus, the realization of nonfluorinated air-stable semiconductors PDI-8CN2, ADI-8CN2, and NDI-8CN2 (Figure 1) showed that the materials with first reduction potentials ≥ −0.4 V can operate in air without severe device performance degradation, suggesting the presence of an overpotential (i.e., free energy of activation) of ∼0.5−1.0 V.[15−17] Similar overpotential values were also estimated by de Leeuw et al.[11] The present study offers further insight into such overpotential values based on a new class of ladder-type semiconductors, providing key information for the rational design of new n-channel materials with air-stable electron transport.

Exceptionally electron-deficient cyano-functionalized arylenediimides (PDI-8CN2, ADI-8CN2, and NDI-8CN2) represent first-generation examples of thermodynamically air-stable, n-channel semiconductors having high electron mobilites of 0.01−0.64 $cm^2/V\cdot s$ and I_{on}/I_{off} ratios of 10^4-10^7.[18,19] However, when these materials are processed from solution, they exhibit appreciably lower FET performance ($\mu_e \approx 10^{-3}$ $cm^2/V\cdot s$) reflecting measurable microstructural irregularities in the solution-processed films.[20] Recently, somewhat higher solution-derived PDI-8CN2 film mobilities of 0.02−0.1 $cm^2/V\cdot s$ were achieved by device structure and deposition process optimization.[21,22] Additionally, a solution-processable dicyanomethylene-substituted terthienoquinoid derivative (DCMT, Figure 1) was reported to exhibit $\mu_e \approx 0.16$ $cm^2/V\cdot s$ in air; however, it suffers from a low I_{on}/I_{off} ratio ($\sim 10^3-10^4$) and μ_e drops to ∼0.01 $cm^2/V\cdot s$ over time in ambient.[23] In contrast to these molecular results, the only reported n-channel polymer with air-stability is the ladder-type polymer, BBL (Figure 1; $\mu_e \approx 0.03$ $cm^2/V\cdot s$ and $I_{on/off} = 10^5$).[24] The low solubility of this material requires aggressive Lewis acid solutions ($GaCl_3$, methanesulfonic acid) for dissolution, which is unattractive for large-scale applications. Previously, well-known p-channel polymeric semiconductors were shown to exhibit n-channel behavior after dielectric surface treatment to remove hydroxyl (−OH) groups; however, the resulting TFTs only operate under vacuum and become inactive in the presence of O_2 and moisture.[25] Therefore, the paucity of air-stable n-channel polymers which can be processed from conventional organic solvents has hindered utilizing the superior rheological properties of polymers in printing processes. This largely reflects the synthetic challenges in optimizing the delicate balance between solubility and efficient solid-state packing. Additionally, the development of air-stable n-channel polymers is of importance in the fundamental understanding of OFET charge transport.[26] Achieving high performance air-stable n-channel polymers requires the design of monomeric building blocks possessing several key characteristics: (i) structural planarity for efficient charge delocalization/solid-state packing, (ii) solubility for processibility, (iii) electron-deficiency for electron injection/conduction in ambient, and (iv) terminal reactive functionalities for efficient polymerization processes. To date, the incorporation of the aforementioned air-stable monomers into polymeric backbones has not yielded macromolecule-based n-channel OFETs which operate in air, largely because potential polymerization sites are occupied by either electron-withdrawing functionalities (−CN) or substituents with poor polymerization reactivities (−F).

A critical goal for organic CMOS is to realize solution-processable molecular/polymeric semiconductors possessing high n-channel mobility (≥0.1 $cm^2/V\cdot s$) and air stability along with good OFET current modulation ($\geq 10^5$) characteristics. Semiconductors exhibiting these characteristics would be excellent candidates for practical OTFT applications, reflecting the intrinsic technological attractions of solution-processable materials, such as facile film formation, compatibility with low-cost manufacturing, and direct-write printing techniques on flexible plastic substrates. These considerations prompted us to seek new electron-deficient (low-lying LUMO) molecular building blocks and their corresponding polymers based on ladder-type (bis)-indenofluorene architectures. Here we present a full account of the synthesis and characterization of a new family of ladder-type molecules and polymers (**1**−**12** and **P1**−**P13**, Figures 2 and 3) in which highly electron-deficient carbonyl and dicyanovinylene groups are introduced into planar indenofluorene and bisindenofluorene structures along with solubilizing alkyl chains. The design rationale explored here and embodied in constituents **1**-**12** is: (i) highly π-conjugated planar cores to facilitate efficient π-electron delocalization and to favor good intermolecular π−π stacking,[27] (ii) electron-withdrawing carbonyl and dicyanovinylene functionalities to depress LUMO energies, which is crucial for achieving electron transport and air-stability,[28] (iii) alkyl side chains (n-$C_{12}H_{25}$) to increase core solubility without disrupting backbone π-conjugation,[29] and (iv) aryl bromide functionalities at the molecular termini to access

(15) Wang, Z.; Kim, C.; Facchetti, A.; Marks, T. J. *J. Am. Chem. Soc.* **2007**, *129*, 13362–13363.
(16) Jones, B. A.; Ahrens, M. J.; Yoon, M. H.; Facchetti, A.; Marks, T. J.; Wasielewski, M. R. *Angew. Chem., Intl. Ed.* **2004**, *43*, 6363–6366.
(17) Schmidt, R.; Ling, M. M.; Oh, J. H.; Winkler, M.; Könemann, M.; Bao, Z.; Würthner, F. *Adv. Mater.* **2007**, *19*, 3692–3695.
(18) Jones, B. A.; Facchetti, A.; Marks, T. J.; Wasielewski, M. R. *Chem. Mater.* **2007**, *19*, 2703–2705.
(19) Jones, B. A.; Facchetti, A.; Wasielewski, M. R.; Marks, T. J. *J. Am. Chem. Soc.* **2007**, *129*, 15259–15278.
(20) Lee, Y.-L.; Hsu, H.-L.; Chen, S.-Y.; Yew, T.-R. *J. Phys. Chem. C* **2008**, *112*, 1694–1699.
(21) Yan, H.; Zheng, Y.; Blache, R.; Newman, C.; Lu, S.; Woerle, J.; Facchetti, A. *Adv. Mater.* **2008**, *9999*, 1–6.
(22) Yoo, B.; Jones, B. A.; Basu, D.; Fine, D.; Jung, T.; Mohapatra, S.; Facchetti, A.; Dimmler, K.; Wasielewski, M. R.; Marks, T. J.; Dodabalapur, A. *Adv. Mater.* **2007**, *19*, 4028–4032.
(23) Handa, S.; Miyazaki, E.; Takimiya, K.; Kunugi, Y. *J. Am. Chem. Soc.* **2007**, *129*, 11684–11685.
(24) Babel, A.; Jenekhe, S. A. *J. Am. Chem. Soc.* **2003**, *125*, 13656–13657.
(25) Chua, L. L.; Zaumseil, J.; Chang, J. F.; Ou, E. C. W.; Ho, P. K. H.; Sirringhaus, H.; Friend, R. H. *Nature* **2005**, *434*, 194–199 (The work function of a gold eldectrode may vary between 4.6 and 5.2 eV depending on the deposition technique and the amount of contamination).
(26) Hutchison, G. R.; Ratner, M. A.; Marks, T. J. *J. Am. Chem. Soc.* **2005**, *127*, 16866–16881.
(27) Woody, K. B.; Bullock, J. E.; Parkin, S. R.; Watson, M. D. *Macromolecules* **2007**, *40*, 4470–4473.
(28) Thompson, B. C.; Kim, Y.-G.; McCarley, T. D.; Reynolds, J. R. *J. Am. Chem. Soc.* **2006**, *128*, 12714–12725.
(29) Anthony, J. E. *Chem. Rev.* **2006**, *106*, 5028–5048.

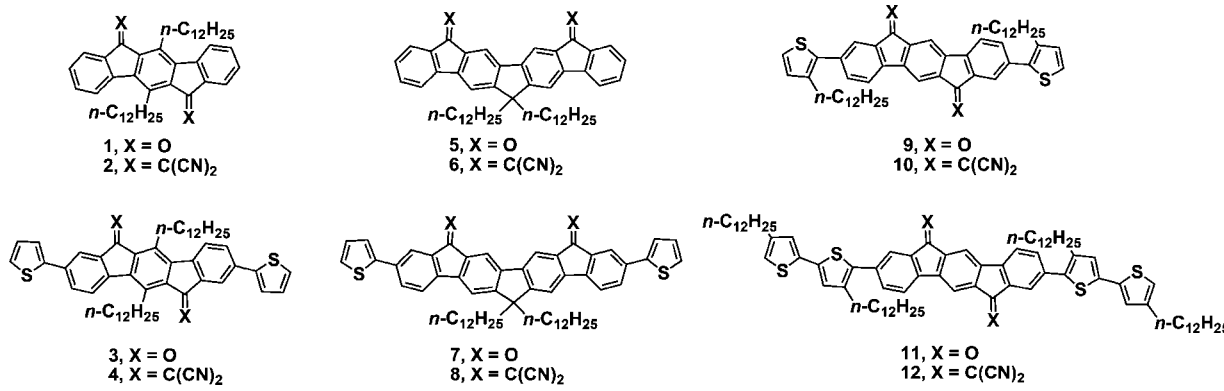

Figure 2. Structures of ladder-type (bis)indenofluorene-based compounds **1**−**12**.

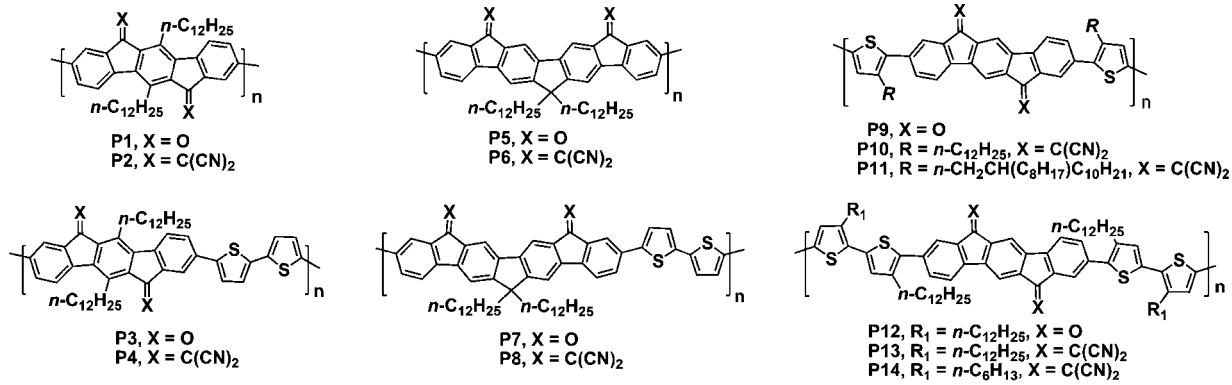

Figure 3. Structures of ladder-type (bis)indenofluorene-based homo- and copolymers **P1**−**P14**.

the corresponding polymers via efficient Stille and Yamamoto polymerization protocols.

In recent preliminary reports, we described synthetic approaches to compounds **1**, **2**, **5**, **6**, and **10**.[30,31] Limited initial FET measurements revealed that two of these materials are n-channel semiconductors with electron mobilities of 0.002−0.16 $cm^2/V.s$, which represented the first report of bis(indenofluorene)-based semiconductors in OFETs. Here we report in full on the synthesis and characterization of seven new polymer building blocks (**3**, **4**, **7**, **8**, **9**, **11**, and **12**) to further elucidate architecture-electronic structure relationships and their effects on OFET response. The suitability of these building blocks for the corresponding polymeric semiconductors is then investigated by conversion of dibromo-functionalized monomers **M1**−**M6** to solution-processable polymers **P2**, **P3**, **P4**, **P6**, **P7**, **P8**, **P12**, **P13**, and **P14** via conventional/microwave-assisted Stille and Yamamoto polymerization protocols. All of the new compounds and polymers are characterized by optical spectroscopy, photoluminescence, cyclic voltammetry, differential scanning calorimetry, and thermogravoimetric analysis. Corresponding thin films are studied by X-ray diffraction, AFM, and FET measurements. For this new family of ladder-type molecules and polymers, through modifications of core structures and functionalities, HOMO/LUMO energetics can be finely tuned (Δ = 0.1 eV) over 1.0 eV, allowing determination of the MO energetic windows governing carrier polarity and environmental stability. In the present series of thin films having different crystallinities, orientations, and morphologies, it is shown that OFET air stability is principally governed by LUMO energetics with minimal contribution from the film microstructure. The onset LUMO energy for electron stabilization during charge transport is estimated as −4.1 to −4.0 eV, which indicates that an overpotential of 0.9−1.0 eV is operative for reaction of the organic π-anions with O_2/H_2O. Depending on the relative HOMO and LUMO energy positions versus source and drain electrode work functions, p-channel (μ_h up to 0.01 $cm^2/V\cdot s$), ambipolar (μ_e up to 0.01 $cm^2/V\cdot s$, μ_h up to 0.006 $cm^2/V\cdot s$), or n-channel behavior (μ_e up to 0.02 $cm^2/V\cdot s$) is observed under vacuum and/or ambient. For semiconductors with sufficiently low LUMO energies, air-stable n-channel behavior with mobilities up to 0.16 $cm^2/V\cdot s$ is realized with very high on/off ratios of 10^7−10^8, representing some of the most favorable FET performance metrics achieved to date for n-channel, solution-processed semiconductors in ambient. Furthermore, construction of donor−acceptor structures affords low band gap materials (1.36−1.40 eV) with charge-injection accessible HOMO and LUMO energies, resulting in solution-processed film electron and hole mobilities of 10^{-3}−10^{-4} $cm^2/V\cdot s$ and I_{on}/I_{off} ratios of $\sim 10^4$, including the first examples of molecular and polymeric ambipolar semiconductors operating in air. Correlated density functional theory calculations focus on the effects of carbonyl and dicyanovinylene substituents, π-conjugated core dimensions, and thiophene addition on molecular/device electronics, and provide detailed insight into intrinsic charge transport and carrier polarity characteristics.

Results

Synthesis. The syntheses of (bis)indenofluorene-based compounds **1**−**12** and monomers **M1**−**M6** are shown in Schemes 1−3 in which acid-catalyzed intramolecular Friedel−Crafts

(30) Usta, H.; Facchetti, A.; Marks, T. J. *Org. Lett.* **2008**, *10*, 1385–1388.
(31) Usta, H.; Facchetti, A.; Marks, T. J. *J. Am. Chem. Soc.* **2008**, *130*, 8580–8581.

Scheme 1. Synthesis of Indenofluorene-Based Compounds **1**−**4** and Monomers **M1** and **M2**

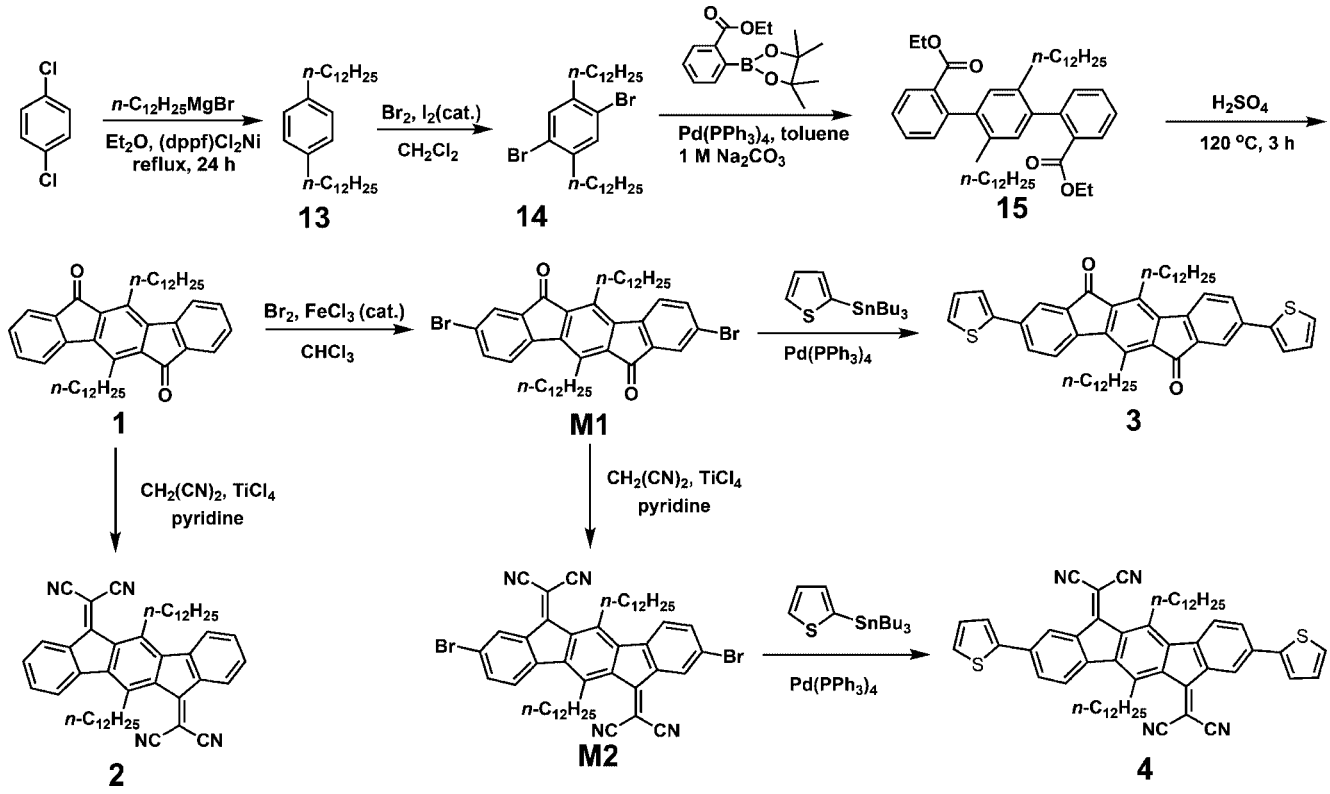

acylations are key steps in forming the ladder-type structures with electron-deficient carbonyl functionalities. As shown in Scheme 1, Kumada coupling of *n*-dodecylmagnesium bromide with 1,4-dichlorobenzene affords 1,4-di-*n*-dodecylbenzene (**13**) in 83% yield, which is then selectively brominated in CH_2Cl_2 under rigorous exclusion of light to afford 2,5-dibromo-1,4-di-*n*-dodecylbenzene (**14**) in 75% yield. Suzuki coupling of **14** with 2-(ethoxycarbonyl)phenylboronic acid pinacol ester gives compound **15** as a colorless oil in 45% yield. The moderate yield obtained for this Suzuki coupling is due to the presence of an electron-withdrawing group (ethyl ester) in the boronic ester reagent, which is known to decrease Suzuki coupling yields.[32] Double intramolecular Friedel−Crafts acylation is next achieved by treatment of diester **15** with concentrated sulfuric acid at 120 °C for 3 h. Indenofluorenedione product **1** is isolated as an orange solid in 93% yield. Compound **1** is then regioselectively brominated at positions 2 and 8 using $FeCl_3/Br_2$ with rigorous exclusion of light to afford monomer **M1** in 85% yield. Subsequent Knoevenagel condensation of **M1** and **1** to form dimalononitrile compounds **2** and **M2**, respectively, is achieved in 45−50% yield using excess malononitrile along with pyridine and $TiCl_4$. Compounds **3** and **4** are obtained via Stille coupling of **M1** and **M2** with 2-tributylstannylthiophene in 50% yield and 60% yield, respectively using $Pd(PPh_3)_4$ as the catalyst.

The syntheses of the bisindenofluorene-based compounds **5**−**8**, **M3**, and **M4** are depicted in Scheme 2. Fluorene boronic ester **16** is synthesized in 90% yield starting from 2,7-dibromo-9,9-didodecylfluorene, which is double-lithiated with *t*-butyllithium and subsequently reacted with 2-isopropoxy-4,4,5,5-tetramethyl[1,3,2]dioxaborolane. Compound **17** is prepared by Suzuki coupling of **16** with methyl 2-iodo-benzoate in high yield (96%). The high yield obtained for this Suzuki coupling reaction is attributed to the fact that the arylhalide is in an ortho position relative to an electron-withdrawing group (methyl ester), which increases the yield through more favorable oxidative-addition processes during the reaction.[33] Treatment of **17** with concentrated sulfuric acid at 165 °C for 3 h induces double intramolecular Friedel−Crafts acylation, yielding bisindenofluorene diketone **5**. The yield obtained for this ring closure is 70%, with high selectivity at each reaction site (84%). Compound **5** is then brominated using $FeCl_3/Br_2$ with rigorous exclusion of light to afford monomer **M3** in 80% yield. Knoevenagel condensation of **5** and **M3** with malononitrile and piperidine as the base then affords **6** and **M4** in 65−70% yield as purple solids. Subsequent Stille coupling of **M3** and **M4** with 2-tributylstannylthiophene using $Pd(PPh_3)_4$ as the catalyst yields compounds **7** (65% yield) and **8** (70% yield), respectively.

As shown in Scheme 3, Suzuki coupling of 1,4-benzenediboronic acid dipinacol ester with methyl 5-bromo-2-iodobenzoate yields compound **18** (89% yield). Intramolecular Friedel−Crafts acylation of **18** is achieved by H_2SO_4 treatment at 120 °C to give compound **19** (91% yield). $Pd(PPh_3)_2Cl_2$-catalyzed Stille coupling of **19** and 2-tributylstannyl-3-dodecylthiophene (**22**) in DMF then yields compound **9** (35% yield), which undergoes reaction with excess malononitrile in the presence pyridine and $TiCl_4$ to afford **10** in 40% yield. Polymer building block **M5** is prepared in 95% yield by bromination of compound **9**, and subsequent Knoevenagel condensation with malononitrile yields **M6** in 45% yield. Compound **11** is obtained by the Stille coupling of **19** with 5-tributylstannyl-4,4′-didodecyl-2,2′-bithiophene (**28**) in 45% yield. Knoevenagel condensation of **11** then yields **12** in 50% yield. The syntheses of the thiophene-

(32) Abraham, M. H.; Grellier, P. L. In *Chemistry of the Metal−Carbon Bond*; Hartley, F. R., Patai, S., Eds.; John Wiley: New York, 1985; p 115.

(33) Suzuki, A. *Proc. Jpn. Acad. Ser. B* **2004**, *80*, 359–371.

Scheme 2. Synthesis of Bisindenofluorene-Based Compounds **5**−**8** and Monomers **M3** and **M4**

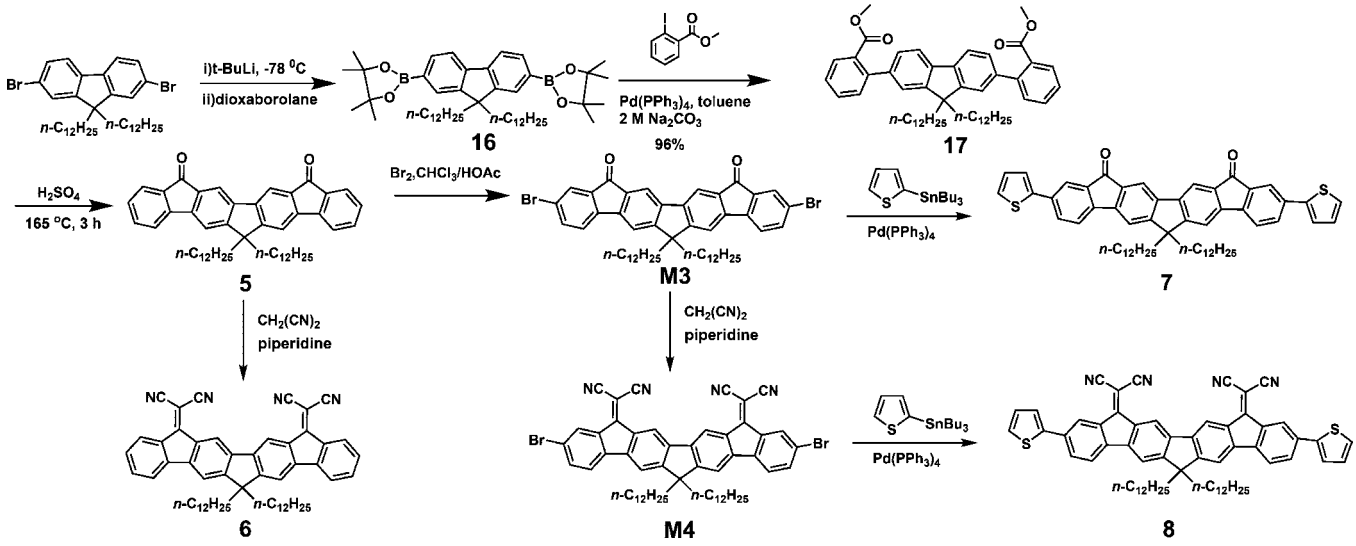

Scheme 3. Synthesis of Indenofluorene-Based Compounds **9**−**12** and Monomers **M5** and **M6**

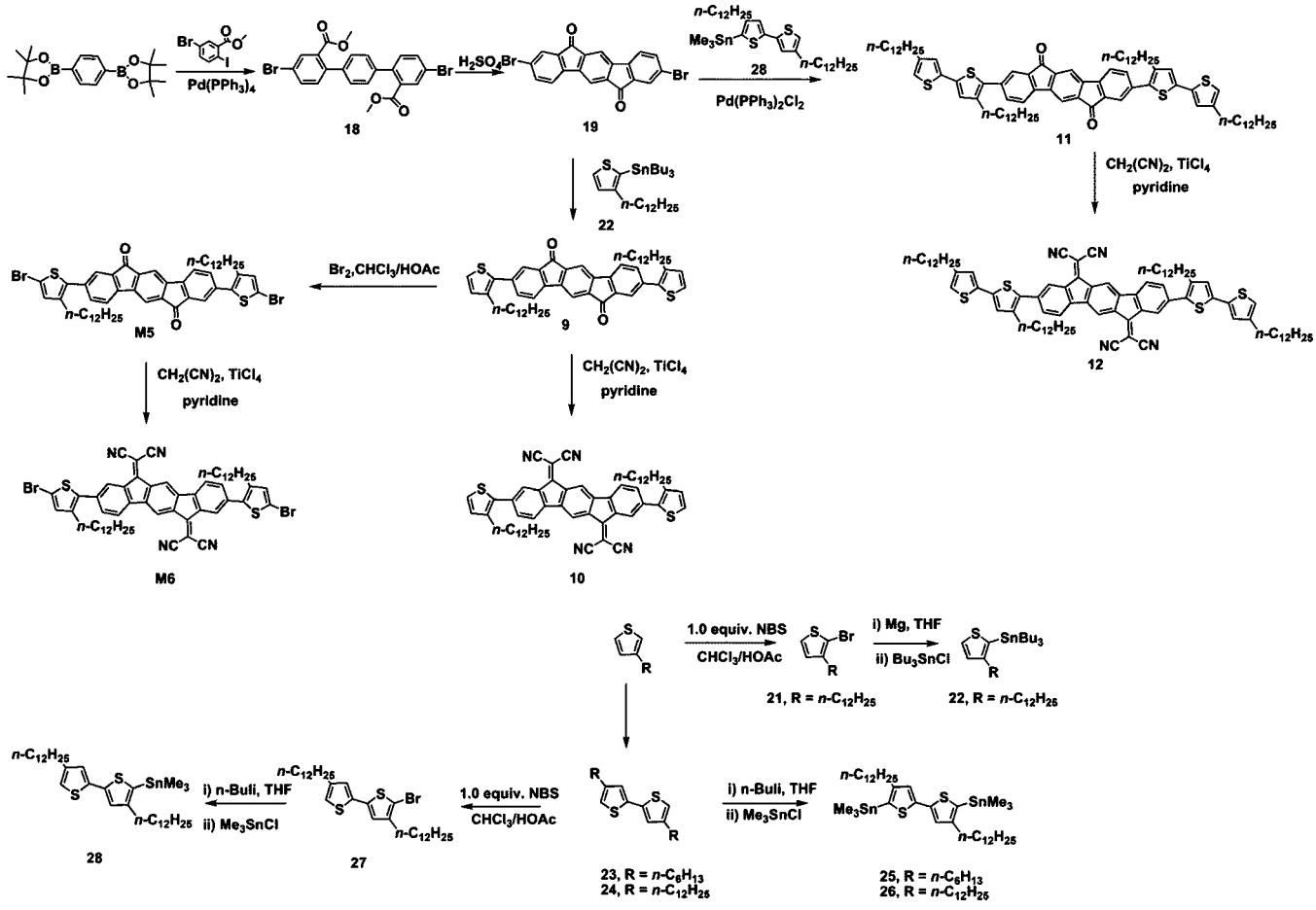

based compounds **21**−**28** are achieved through selective bromination and stannylation reactions. Oxidative coupling of the monolithiated derivatives of 3-hexylthiophene and 3-dodecylthiophene in the presence of $CuCl_2$ affords **23** and **24**, respectively. Monobromination of **23** followed by monostannylation affords compound **28** in 90% yield. Selective bromination of 3-dodecylthiophene at position 2 and subsequent stannylation then affords **22** in 90% yield. Compounds **25** and **26**, which are used as comonomers in the polymerization reactions, are obtained from **23** and **24**, respectively, via double lithiation with *n*-BuLi, followed by the addition of Me_3SnCl in 80% and 85% yields, respectively.

Compounds **1**−**12** and monomers **M1**−**M6** are freely soluble in common organic solvents ($CHCl_3$, CH_2Cl_2, THF, toluene) which allows convenient purification by flash column chromatography. This is a significant advantage over many reported semiconductors which have poor solubilities and require high-temperature vacuum sublimation techniques for purification. All

of the present compounds were characterized by ^{1}H and ^{13}C NMR, elemental analysis, IR, and mass spectroscopy (EI/ESI/MALDI-TOF).

During the synthesis of **6** from **5** via Knoavegel condensation, excess malononitrile with a piperidine base in DMF is used and the product is isolated in 65% yield. In contrast, a similar condensation for compound **1** proceeds sluggishly under the same reaction conditions, and requires a Lewis acid such as $TiCl_4$ for reasonable yields. This requirement was at first thought to result from increased steric repulsion at each reaction site of **1**; however, the same difficulty for sterically less hindered **9** suggests that the highly electron-deficient nature of the indenofluorene core formed in this reaction ($E_{1/2}^{red\text{-}1} = -0.14$ V vs SCE, vide infra) impedes the second condensation step, reflecting the significant demands of forming of such unusually electron-deficient cores.[34] In order to synthesize the bithiophene-terminated ladder-type structures, dibromo-functionalized compounds **M1**−**M6** were first coupled with 5-tributylstannyl-2,2′-bithiophene, resulting in products with poor solubilities which prevented their further purification and characterization. The poor solubilities of these compounds are attributed to the absence of solubilizing groups on the outer thiophene units, which would otherwise compensate for the diminished solubility arising from molecular core extension. In contrast, monothiophene-terminated compounds **3**, **4**, **7**, and **8** are freely soluble in conventional organic solvents as a result of optimum π-conjugated core extension (i.e., a single thiophene unit at either end) while maintaining high solubility. For the sterically encumbered Stille couplings of **19** with compounds **22** and **28**, the $Pd(PPh_3)_4$/toluene catalyst system does not yield any significant coupling product; however, $Pd(PPh_3)_2Cl_2$ in DMF is found to be more effective and the desired products are obtained in reasonable yields (35−40%), likely attributable to the higher turnover frequencies of more coordinatively unsaturated $Pd(PPh_3)_2X_2$ species.[33,35] For this particular Stille coupling, similar yields (∼35%) are obtained for thiophenes with "swallow tail" (2-octyldodecyl) and linear (*n*-dodecyl) alkyl substituents, indicating that the reaction is not particularly sensitive to alkyl substituent encumberance on the thiophene reagent.

To optimize the delicate balance between solubility and thin film microstructural order, alkyl chain substituents on indenofluorene-based compound **9** and bisindenofluorene-based compound **6** were iteratively adjusted. Thus, *n*-hexyl- and *n*-octyl-substituted derivatives of compounds **5** and **6** were synthesized to examine the effect of alkyl chain on thin-film microstructure and FET performance. A "swallow tail" (C_8,C_{12}) substituted derivative of **10** was also synthesized and found to be significantly more soluble than its linear alkyl ($-n$-$C_{12}H_{25}$) counterpart. In addition, the copolymerization of monomer **M6** with bistannylated derivatives of 4,4′-didodecyl-2,2′-bithiophene and 4,4′-dihexyl-2,2′-bithiophene was also examined to improve polymer solubility.

Polymers **P1**−**P14** are synthesized according to Scheme 4. In general, homopolymers **P1**, **P2**, **P5**, **P6**, **P9**, **P10**, and **P11** are synthesized via Yamamoto polycondensations using $Ni(COD)_2$ as the catalyst and bipyridine + COD as cocatalysts. Copolymers are synthesized via conventional or microwave-assisted Stille polycondensations between the dibromo-functionalized reagents **M1**−**M6** and bistannylbithiophene compounds. Physicochemical properties of the present polymers are summarized in Table 2. Homopolymers **P1**, **P5**, **P9**, **P10**, and **P11** have limited solubilities which prevents further purification and characterization. Halting the polymerization process at early stages of the reaction does not yield soluble polymeric products. However, dicyanovinylene-functionalized homopolymers **P2** and **P6** are freely soluble in common organic solvents which may reflect the large local dipole moments (vide infra) of the monomeric units which enhance solvation. Interestingly, we find that bithiophene copolymers **P3**, **P4**, **P7**, and **P8** are more soluble (up to 40% by mass) than corresponding homopolymers **P1**, **P2**, **P5**, and **P6**, as a result of an increase in the degrees of rotational freedom which reduces backbone rigidity and increases solubility.[36]

Thermal Properties. The thermal properties of the present compounds **1**−**12** and polymers **P1**−**P14** were investigated by thermogravimetric analysis (TGA), differential scanning calorimetry (DSC), and conventional melting point determinations. Figure 4 shows the thermal scans, and data are collected in Tables 1 and 3. For TGA, a 5% mass loss is defined as the thermolysis threshold. Thermolysis onset temperatures for all compounds **1**−**12** and polymers **P1**−**P15** are above 350 °C, indicative of good thermal stabilities, which allow thin film crystallinity and microstructure analysis over a broad range of annealing temperatures, 50−300 °C. The observed melting points for compounds **1**−**12** are within ∼0−5 °C of the values obtained by DSC scans. We find that molecular and macromolecular structural details have considerable influence on thermal phase transitions via the qualitative interplay of two intermolecular forces, $\pi-\pi$ stacking interactions, and alkyl chain interdigitations. Dicyanovinylene-functionalized compounds **6**, **8**, **10**, and **12** exhibit much higher melting temperatures than the corresponding carbonyl-functionalized structures **5**, **7**, **9**, and **11**. The increase of ∼80−114 °C doubtless reflects substantial differences in cohesive energetics of the solid state intermolecular interactions. For each pair of compounds (**5/6**, **7/8**, **9/10**, and **11/12**), considering the similar core sizes and small increases in molecular weight (∼96 amu), the melting point increases are likely a combined result of larger local/molecular dipole moments in the dicyanovinylene-functionalized compounds versus their carbonyl-functionalized counterparts and enhanced molecular donor−acceptor characteristics which should enhance intermolecular cohesion through dipole−dipole and π-π interactions, resulting in more effective solid-state packing.[13] The relative orientation of the dicyanovinylene groups, hence the local dipoles, at each methylene bridge appears to have little effect on the solid-state packing since similar melting point increases are observed for the indenofluorene (dicyanovinylenes syn) and bisindenofluorene (dicyanovinylenes trans) compounds. For compounds **5**−**8**, DFT calculations show that dicyanovinylene functionalization induces a relatively large dipole moment of 13 D compared to carbonyl compounds (7 D), consistent with the experimental results (see more below). On the other hand, because of the C_2-symmetric placement of the dipoles, the total molecular dipole moments are near zero for compounds **1**−**4** and **9**−**12**. Upon conversions **1** → **3** and **2** → **4**, the melting points increase only by 5−10 °C. This small change in melting point upon dicyanovinylene functionalization is probably due to the increased steric repulsions at the methylene bridges which cause significant deviations from core planarity, resulting in poor solid state packing. This suggestion is further confirmed by

(34) Frank, W.; Gompper, R. *Tetrahedron Lett.* **1987**, *28*, 3083–3086.
(35) Trouillet, L.; Nicola, A. D.; Guillerez, S. *Chem. Mater.* **2000**, *12*, 1611–1621.
(36) Crouch, D. J.; Skabara, P. J.; Lohr, J. E.; McDouall, J. J. W.; Heeney, M.; McCulloch, I.; Sparrowe, D.; Shkunov, M.; Coles, S. J.; Horton, P. N.; Hursthouse, M. B. *Chem. Mater.* **2005**, *17*, 6567–6578.

Scheme 4. Synthesis of (Bis)indenofluorene-Based Homo- and Copolymers **P1**−**P15**

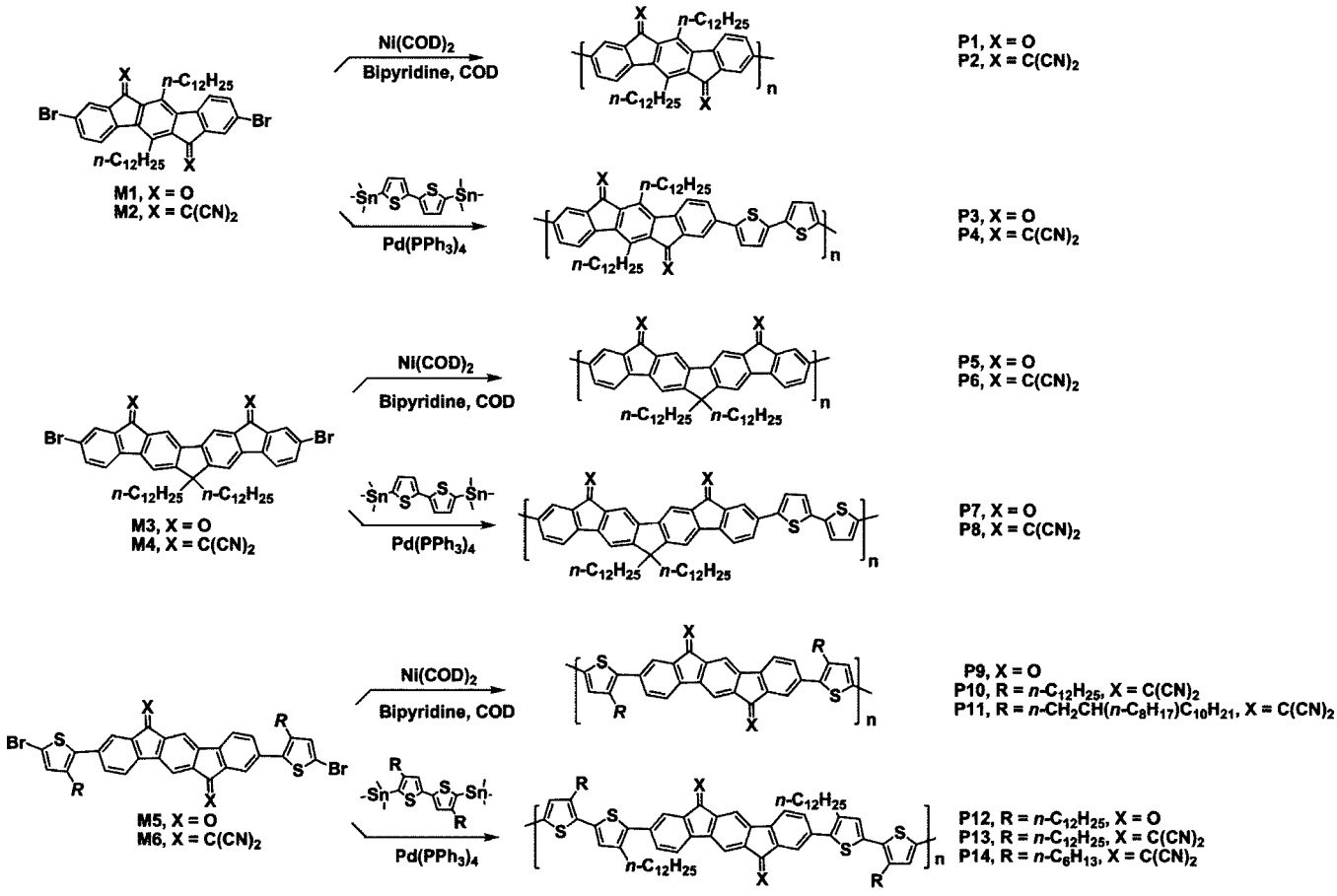

single-crystal structures and DFT calculations which show that while indenofluorene cores in compounds **1** and **9** have highly planar cores with small twist angles of ∼0°, upon dicyanovinylene functionalization, the core in compound **2** twists significantly from planarity (Δ = ∼21°), while core planarity is preserved in compound **10** (Figures 5 and 9; see more below).

Compounds **3**, **4**, **7**, and **8**, having additional thiophene units at the molecular termini, have higher melting temperatures (ΔT_{mp} ≈ 40−100 °C) than their indenofluorene/bisindenofluorene counterparts (**1**, **2**, **5**, and **6**), reflecting the collective effect of increased molecular weight, extended effective π-conjugation, and enhanced donor−acceptor interactions as a result of introducing thiophene donors into electron-deficient indenofluorene/bisindenofluorene acceptor cores. The only exceptions here are thiophene-terminated compounds **11** and **12** in which melting points decrease versus **9** and **10**, respectively. This depression in melting points argues that the contribution of additional alkyl chains ($C_{12}H_{25}$) on the outer thiophene rings to the overall intermolecular cohesive forces via alkyl chain interactions is weaker than the $\pi-\pi$ stacking interactions between the cores.

To further investigate thermal phase transitions, DSC scans were performed at heating and cooling rates of 5 °C/min under N_2, and collected in the second cycle. All of the present compounds exhibit reversible thermal features in all scans, in accord with the aforementioned excellent thermal stabilities. In the heating cycles of **5** and **7**, both exothermic features (93 °C for **5**; 85 °C for **7**) and endothermic peaks (138 °C/144 °C for **5**; 177 °C/188 °C for **7**) are observed, which was previously attributed to LC characteristics in qualitatively similar flurorene-based compounds.[37] In contrast, compounds **6**, **8**, and **10** exhibit multiple DSC thermal transitions with endotherms located at 240 °C/251 °C for **6**, 271 °C/279 °C for **8**, and 93 °C/234 °C for **10**, and exotherms located at 164 °C for **6**, 243 °C for **8**, and 200 °C/74 °C for **10**. As shown in Figure 4, polarized optical micrographs acquired during the slow cooling process (0.1 °C/min) of compounds **7** and **10** reveal the separation of anisotropic nematic and mosaic-like smectic liquid crystal phases, respectively at $T < 180-225$ °C, and spherulite-like crystalline phases exhibiting birefringences at lower temperatures ($T < 80-90$ °C). This thermal feature at 93 °C is attributed to a crystal-to-crystal phase transition which is also observed in the corresponding thin films upon annealing (vide infra). The aforementioned intermolecular forces not only yield high melting points for dicyanovinylene functionalized compounds, but also enforce long-range order, which is reflected here by the presence of an LC phase. Considering the importance of molecular/macromolecular order and $\pi-\pi$ interactions in determining charge carrier mobility, this kind of long-range ordering is crucial to realizing maximum OFET performance through alignment of the semiconducting molecules via thermally optimized processing.

The thermal properties of the present polymers were also investigated by DSC. Copolymers **P3**, **P7**, **P8**, **P12**, **P13**, and **P14** exhibit endotherms at 260, 280, 310, 322, 330, and 335 °C on the heating cycle. Corresponding exotherms are observed at 290 and 280 °C for **P8** and **P12**, respectively. Polymer **P6** exhibits a glass transition at 120 °C with an endothermic peak

(37) Lim, E.; Jung, B. J.; Lee, J.; Shim, H. K.; Lee, J. I.; Yang, Y. S.; Do, L. M. *Macromolecules* **2005**, *38*, 4531–4535.

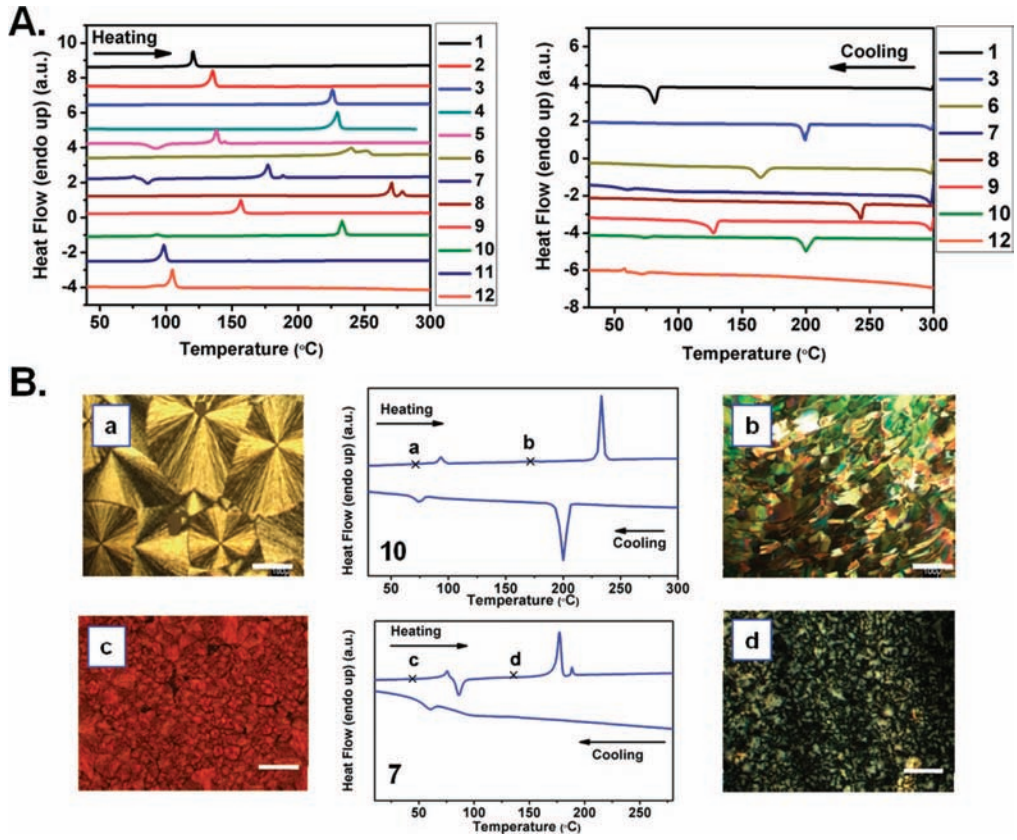

Figure 4. (A) Differential scanning calorimetry (DSC) of the compounds **1**−**12** at a temperature ramp of 5 °C/min under N_2. (B) Optical images of compounds **7** and **10**, taken under 90° cross-polarization conditions as a function of temperature. Scale bars denote 100 μm.

Table 1. Summary of Thermal, Optical Absorption/Emission, and Electrochemical Properties of Compounds **1**−**12**, and Corresponding Estimated Frontier Molecular Orbital Energies

compd (nm)	mp (°C)	T_{DSC} (°C)[a] heating (cooling)	T_{TGA}[b] (°C)	$E_{sol.}^{red-1/2}$ (V)[c]	E_{film}^{red-1} (V)[d]	E_{film}^{ox-1} (V)[d]	E_g^{CV} (eV)[d]	E_{LUMO} (eV)[e]	E_{HOMO} (eV)[f]	λ_{abs}^{soln} (nm) (E_g (eV))[g]	λ_{em}^{sol} (nm)[h]	$\lambda_{abs}^{thin-film}$ (nm) (E_g(eV))[k]	$\lambda_{em}^{thin-film}$
1	122	121 (82)	380	−0.77	−0.73	+1.30	2.03	−3.67	−5.95	368, 484 (2.28)	590	375, 533 (2.16)	561, 587
2	136	135 (N.A.)	400	−0.14	−0.15	+1.50	1.65	−4.30	−6.16	426, 579 (1.83)	762[i]	423, 576 (1.80)	755[i]
3	220	225 (200)	395	−0.90	−0.73	+1.10	1.83	−3.54	−5.54	374, 537 (2.02)	623	364, 620 (1.80)	530, 570
4	225	229 (N.A.)	360	−0.24	−0.20	+1.30	1.50	−4.20	−5.74	430, 661 (1.54)	770[i]	440, 690 (1.50)	750[i]
5	138	138,144 (N.A.)	375	−1.20	−1.10	+1.26	2.36	−3.24	−5.68	365, 455 (2.44)	540	372, 490 (2.34)	551
6	252	240, 251 (164)	385	−0.53	−0.54	+1.30	1.84	−3.91	−5.86	378, 513 (1.95)	768[i]	385, 610 (1.86)	760[i]
7	180	177,188 (60)	405	−1.25	−1.25	+1.10	2.35	−3.19	−5.50	394, 472 (2.31)	545	406, 531 (2.16)	569
8	280	271, 279 (243)	410	−0.72	−0.70	+1.15	1.85	−3.72	−5.52	400, 576 (1.80)	785[i]	410, 652 (1.72)	720[i]
9	152	155 (128)	420	−0.74	−0.72	+1.25	1.97	−3.70	−5.75	377, 525 (2.05)	619	365, 594 (1.89)	640
10	232	93, 234 (200, 74)	403	−0.12	−0.20	+1.40	1.60	−4.32	−5.84	418, 653 (1.52)	780[i]	412, 759 (1.50)	730[i]
11	96	98 (N.A.)	382	−0.85	−0.80	+1.05	1.85	−3.59	−5.53	394, 540 (1.94)	670	380, 611 (1.86)	670
12	103	105 (73)	370	−0.20	−0.30	+1.30	1.60	−4.20	−5.64	410, 711 (1.44)	785[i]	378, 738 (1.40)	740[i]

[a] From DSC scans under nitrogen at a scan rate of 5 °C/min. [b] Onset decomposition temperature measured by TGA under nitrogen. [c] 0.1 M $Bu_4N^+PF_6^-$ in THF (vs SCE) at a scan rate of 100 mV/s. [d] As thin-film with 0.1 M $Bu_4N^+PF_6^-$ in acetonitrile (vs SCE). [e] Estimated from the equation $E_{LUMO} = -4.44$ eV $- E_{sol.}^{red-1/2}$. [f] E_{HOMO} is calculated from $E_g = E_{LUMO} - E_{HOMO}$. [g] From optical absorption in THF, optical band gap is estimated from the low energy band edge of the UV−vis spectrum. [h] From optical emission in THF. [i] Broad, weak emission peak. [k] From optical absorption as spin-coated thin film on glass, optical band gap is estimated from the low-energy band edge of the UV−vis spectrum.

at 260 °C and an exothermic peak at 243 °C. The higher endothermic transition temperature observed for **P8** versus **P6** can be attributed to the presence of the bithiophene comonomer in the former which is known to increase thermal transition temperatures in semiconducting polymers.[1,2]

Optical Properties. Solution/thin-film optical and fluorescence spectra of compounds **1**−**12** and polymers **P1**−**P5** are shown in Figure 6, and optical data are collected in Tables 1 and 2. Due to the presence of multiple absorption transitions and large Stokes shifts, solution and solid state optical band gaps (E_g) were estimated from the low-energy band edges of the optical spectra.[38] The solution-based absorption and emission measurements were carried out at very low concentrations (<10^{-5} M) in a solvent of intermediate dielectric constant (THF, $\varepsilon = 7.6$) to minimize the influence of molecular aggregation and differences in molecular dipole moments (solvents with large dielectric constants can preferentially stabilize polar conformations), revealing the "intrinsic" molecular structural features such as planarity, optical HOMO−LUMO gap, and extent of π-conjugation.[39]

(38) Zhu, Y.; Alam, M. M.; Jenekhe, S. A. *Macromolecules* **2002**, *35*, 9844–9846.

Table 2. Majority Charge Carrier Types, Field-Effect Mobilities (μ), Threshold Voltages (V_T), and Current I_{on}/I_{off} Ratios for Thin Films of Compounds **1**−**12** Fabricated by Spin-Coating/Vacuum-Deposition on OTS-Treated Si/p^+-SiO_2 Substrates.[a]

		vapor deposition (T_D = 70 °C)			vapor deposition (T_D = 110 °C)			solution-processed		
compd	polarity	μ ($cm^2/V \cdot s$)	I_{on}/I_{off}	V_T (V)	μ ($cm^2/V \cdot s$)	I_{on}/I_{off}	V_T (V)	μ ($cm^2/V \cdot s$)	I_{on}/I_{off}	V_T (V)
3	n, p	0.002 (e^-) 2×10^{-4} (h^+)	10^5	+45 (e^-) −50 (h^+)	0.01 (e^-) 6×10^{-4} (h^+)	10^6 10^7	+60 (e^-) −40 (h^+)	0.001 (h^+)	10^4	− 42 (h^+)
4[b]	n (air-stable)	4×10^{-4}	10^4	+10	0.001	10^5	+3	0.0001	10^4	+7
6	n	0.002	10^5	+25	0.006	10^6	+30	0.0004	10^5	+32
7	p	0.6×10^{-3}	10^5	−25	0.001	10^5	−18	0.0001	10^5	−27
8	n	0.004	10^5	+20	0.02	10^6	+20	0.0003	10^4	+25
9	n, p	0.002 (e^-, h^+)	10^4	+50 (e^-) − 32 V (h^+)	0.006 (e^-, h^+)	10^4	+50 (e^-) − 30 (h^+)	0.0002 (e^-, h^+)	10^4	+60 (e^-) − 35 (h^+)
10[b]	n (air-stable)	0.03	10^6	+2	0.16	10^7	+5	0.16	10^8	+5
11	p	−[c]	−[c]	−[c]	−[c]	−[c]	−[c]	0.0001	10^4	−30 (h^+)
12[b]	n, p (air-stable)	−[c]	−[c]	−[c]	−[c]	−[c]	−[c]	0.001 (e^-) 1×10^{-4} (h^+)	10^5	+20 (e^-) −25 (h^+)

[a] The mobility values, threshold voltages, and I_{on}/I_{off} ratios given are the average values for 10 devices with the standard deviations less than 5%. SiO_2 dielectric (300 nm, C_i = 10 nF/cm^2); L = 100 μm, W = 1 mm. Measured in a vacuum probe station. [b] Measured in air. [c] Compound is not vapor deposited due to high molecular weight.

Table 3. Physicochemical Properties (Molecular Weight (M_w, kD), Polydispersity (PD), Melting Temperature (T_m), Crystallization Temperature (T_c), Onset Decomposition Temperature (T_d), Solution (in THF), Film Optical Absorption Maxima, Energy Gaps ($E_{g,op}$, eV)],) and FET Performance Summary (OFET Charge Carrier Mobilities and Current on/off Ratios of Polymers **P1**−**P14**

polym	polym protocol	M_w (PD) (kD)	charge	T_m, T_c[a] (°C)	T_d[c] (°C)	$E_{onset}^{red\text{-}1}$ (V) (LUMO)	$E_{onset}^{ox\text{-}1}$ (V) (HOMO)	E_g^{CV} (eV)	$\lambda_{solution}(E_{g,op})$[d] (nm, eV)	λ_{film} ($E_{g,op}$)[d] (nm, eV)	FET μ ($cm^2/V \cdot s$)	FET I_{on}/I_{off}
P2	Yamamoto	13,250 (1.45)	NA	−[b]	445	−0.12 (−4.32)	1.37 (−5.81)	1.49	460, 600 (1.55)	455, 620 (1.45)	-[b]	-[b]
P3	Stille	11,200 (1.20)	p	260, -[b]	420	−0.80 (−3.64)	0.98 (−5.42)	1.78	401, 497 (1.70)	393, 485 (1.70)	0.001	10^4
P4	Stille	14,200 (1.50)	NA	−[b]	410	−0.29 (−4.15)	1.12 (−5.56)	1.41	465, 680 (1.45)	457, 705 (1.55)	-[b]	-[b]
P6	Yamamoto	12,455 (1.55)	n	272, 243	415	−0.37 (−4.07)	1.31 (−5.75)	1.68	418, 577 (1.99)	405, 587 (1.70)	0.5×10^{-4}	10^4
P7	Stille	9,400 (1.52)	p	280, -[b]	430	−0.90 (−3.54)	0.90 (−5.34)	1.80	426, 514 (2.06)	421, 512 (1.77)	3×10^{-4}	10^4
P8	Stille	10,500 (1.30)	p, n	310, 290	425	−0.60 (−3.84)	1.12 (−5.56)	1.72	456, 661 (1.57)	435, 709 (1.61)	0.5×10^{-4}	10^4
P12	Stille	18,300 (2.50)	p	322, 280	405	−0.82 (−3.62)	0.98 (−5.42)	1.80	420, 560 (1.55)	432, 605 (1.55)	0.01	10^5
P13	Stille	23,273 (3.48)	p, n (air stable)	330, -[b]	415	−0.29 (−4.15)	1.07 (−5.51)	1.36	461, 810 (1.38)	471, 847 (1.36)	2×10^{-4}	10^4
P14	Stille	21,370 (2.95)	p, n (air stable)	335, -[b]	410	−0.27 (−4.17)	1.10 (−5.54)	1.37	460, 808 (1.37)	472, 846 (1.36)	2×10^{-4}	10^4

[a] Melting temperature (T_m) and crystallization temperature (T_c) determined by DSC. [b] Not observed. [c] Onset decomposition temperature measured by TGA under nitrogen. [d] Optical band gap estimated from the low energy band edge in the optical spectrum.

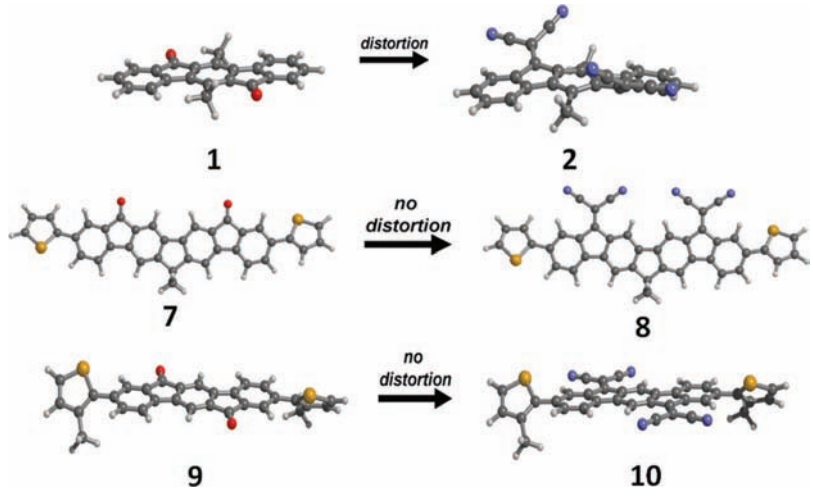

Figure 5. DFT-calculated molecular structures of **1**, **2**, and **7**−**10**.

In THF, the absorption spectra of carbonyl-functionalized compounds **1**, **3**, **5**, **7**, **9**, and **11** exhibit three maxima, two located below 400 nm, and the third at 455−540 nm. The higher energy maxima−368 (**1**), 374 (**3**), 365 (**5**), 394 (**7**), 377 (**9**), and 394 nm (**11**)−correspond to $\pi-\pi^*$ transitions of the indenofluorene and bisindenofluorene backbones, whereas the weaker absorptions at lower energies−484 nm (**1**), 537 (**3**), 455 (**5**), 472 (**7**), 525 (**9**), and 540 nm (**11**)−can be assigned to the symmetry-forbidden n−π^* transitions involving the carbonyl groups.[40] The absolute absorption maxima of all of the bis(indenofluorene)-based compounds are shifted to longer wavelengths by ∼110−140 nm versus that of fluorenone (258 nm in THF).[41] This significant bathochromic shift is consistent with enhanced π-conjugation of the molecular backbone and is

(39) Hernandez, V.; Lopez Navarrete, T. J. *J. Phys. Chem.* **1994**, *101*, 1369–1377.
(40) Oldridge, L.; Kastler, M.; Müllen, K. *Chem. Commun.* **2006**, *8*, 885–887.

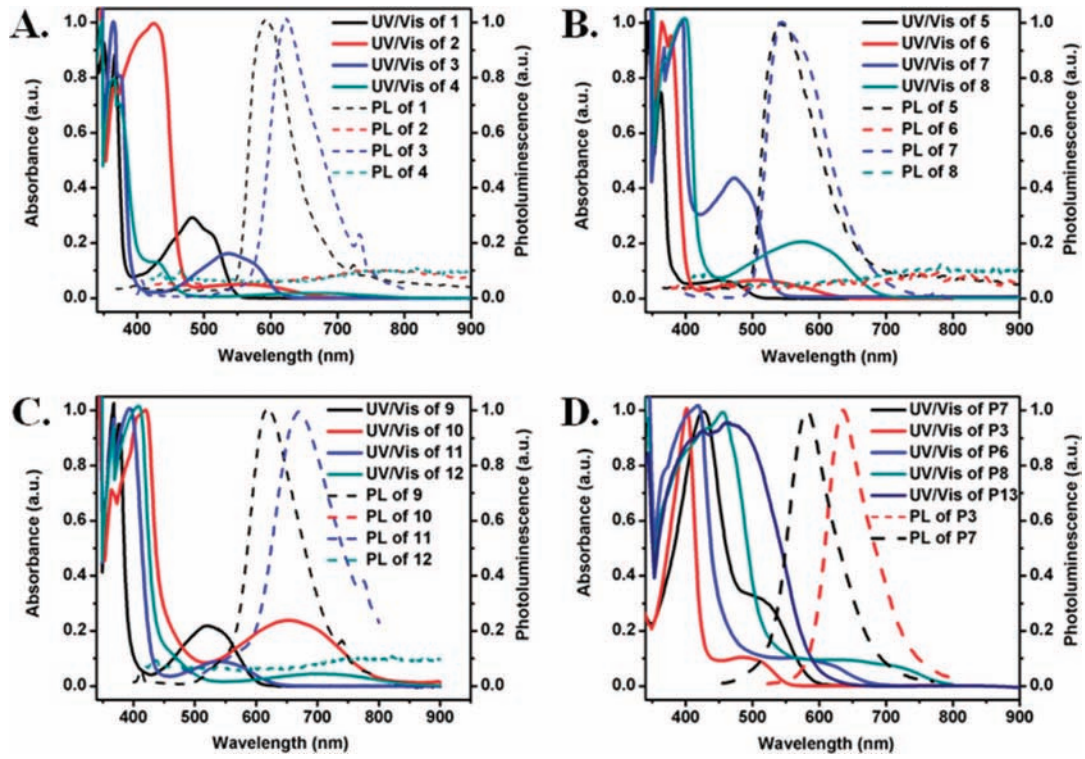

Figure 6. Optical absorption (solid lines) and photoluminescence (dashed lines) spectra of molecules **1**−**12** and polymers **P3**, **P6**, **P7**, **P8**, and **P13** as THF solutions.

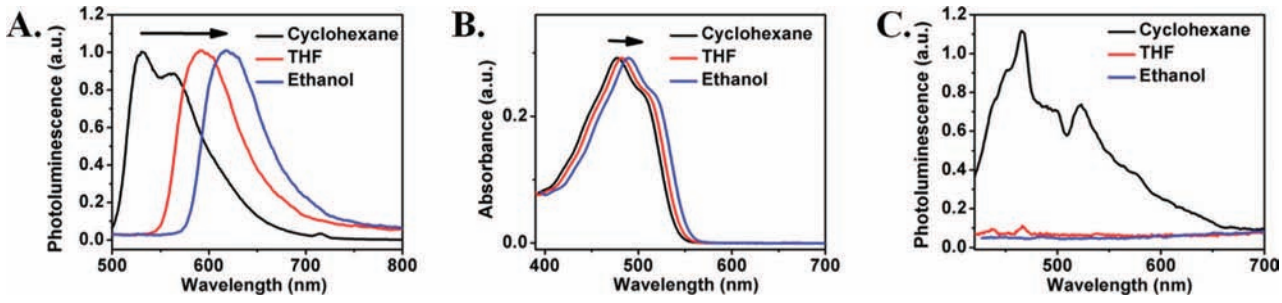

Figure 7. Optical absorption and photoluminescence spectra of molecules **1** (A, B) and **6** (C) in cylohexane, THF, and ethanol solutions.

attributable to the planar, ladder-type structure of these cores embedding two electron-withdrawing carbonyl groups. When the carbonyl functionalities are replaced with dicyanovinylene groups, the high-energy absorption maxima shift to 426 nm for **2**, 430 nm for **4**, 378 nm for **6**, 400 nm for **8**, 418 nm for **10**, and 410 nm for **12**, and long-wavelength absorptions are now observed at 579, 661, 513, 576, 653, and 711 nm for **2**, **4**, **6**, **8**, **10**, and **12**, respectively. The bathochromic shift upon dicyanovinylene functionalization is ∼41−58 nm for the indenofluorene and ∼6−13 nm for the bisindenofluorene core, and is consistent with the reported shifts in similar ladder-type π-conjugated structures.[42,43] Dicyanovinylene functionalization for all of the present compounds results in larger red-shifts in the low-energy absorption maxima (∼60−171 nm) than those of the $\pi-\pi^*$ transitions (∼6−58 nm), suggesting that the optical transitions of the low-energy absorption maxima have significant contributions from the frontier MOs that are primarily localized on the methylene bridges, making them more susceptible to functionalization at these positions. This is consistent with the previous assignment of these transitions as n$-\pi^*$ in character. Although the short-wavelength absorption maxima show negligible solvachromatism, the long-wavelength absorptions exhibit red-shifts ($\Delta\lambda$ = 5−20 nm) with increased solvent polarity (cyclohexane (ε = 2.0) → THF (ε = 7.6) → ethanol (ε = 30.0)), indicating positive solvachromatism (Figure 7). Since blue-shifts are typically expected for n$-\pi^*$ absorptions upon increasing the solvent polarity, the presence of a red-shift suggest that the Franck−Condon excited state ($S_{1(n-\pi^*)}$) has significant polar character. The red-shifts observed upon dicyanovinylene functionalization are attributed to LUMO energetic stabilization arising from the stronger electron-withdrawing nature of the dicyanovinylene versus carbonyl substituent, resulting in band gap contractions from 2.28 to 1.83 eV (**1** → **2**), from 2.02 to 1.54 eV (**3** → **4**), from 2.44 to 1.95 eV (**5** → **6**), from 2.31 to 1.80 eV (**7** → **8**), from 2.05 to 1.52 eV (**9** → **10**), and from

(41) Jaramillo-Isaza, F.; Turner, L. M. *J. Mater. Chem.* **2006**, *16*, 83–89.
(42) Berlin, A.; Zotti, G.; Zecchin, S.; Schiavon, G.; Vercelli, B.; Zanelli, A. *Chem. Mater.* **2004**, *16*, 3667–3676.
(43) Lambert, T. L.; Ferraris, J. P. *J. Chem. Soc., Chem. Commun.* **1991**, 752–754.

1.94 to 1.44 eV (**11** → **12**).[44] These gaps are considerably smaller ($\Delta E_g = 1.75-2.26$ eV) than those of typical nonfunctionalized indenofluorene cores (~3.70 eV), indicative of HOMO and LUMO stabilization with a greater magnitude in the latter—a crucial step toward the development of new air-stable n-channel and ambipolar semiconductors.[45]

The optical absorption spectra of thiophene-terminated compounds **3**, **4**, **7**, **8**, **11**, and **12** exhibit absorption maxima that are red-shifted ($\Delta\lambda_{max} = 6-41$ nm) versus those of (bis)indenofluorene core structures **1**, **2**, **5**, **6**, **9**, and **10**, reflecting the effects of extended core dimensions, enhanced π-electron delocalization, and formation of donor−acceptor type structures upon appending electron-rich thiophenes to the electron-deficient cores. In addition, smaller band gaps ($\Delta E_g = 0.1-0.3$ eV) are observed for thiophene-functionalized molecules (2.02 (**3**), 1.54 (**4**), 2.31 (**7**), 1.80 (**8**), 1.94 (**11**), and 1.44 eV (**12**)) versus the (bis)indenofluorene core structures. These band gap contractions are further confirmed by nonsymmetric increases in the HOMO and LUMO energies with the former being larger (see electrochemical data, vide infra). A similar trend was previously reported for a series of thiophene−phenylene oligomers.[46]

Thin-film optical spectra of the present compounds were recorded on spin-coated films on glass substrates, and data are summarized in Table 1. Although the solution-phase absorption spectra are devoid of significant fine structure, thin-film absorption spectra exhibit vibronic features with peak intervals of 0.15−0.20 eV, corresponding to the typical energies of aromatic C=C bond stretches.[47] This vibronic coupling may reflect molecular planarization in the thin-film phase versus the solution phase in which molecules have greater degrees of structural freedom. The film high-energy absorption maxima are at 363−410 nm which are, except for **9**−**12**, red-shifted by ~10−15 nm versus the corresponding solution absorption maxima. The blue-shifts observed for compounds **9**−**12** suggest significant H-type aggregate coupling between transition dipoles as in the aforementioned thiophene−phenylene series.[46,48] The thin-film absorption maxima follow the same general trends as the solution-phase absorption maxima, indicating similar molecular structure effects on optical features in solution and thin films. In addition, shoulders at longer wavelengths (490−759 nm) appear in the thin-film phase with significant red-shifts of ~27−169 nm, indicating higher planarity of molecular backbone and enhanced molecular ordering in thin-film phase compared to the solution phase. This conclusion is further confirmed by thin-film XRD and AFM data (vide infra).[23,49] In general, the thin film optical band gaps follow trends similar to the solution-phase data, and they are 0.1−0.2 eV smaller than the corresponding solution values, indicating a greater average π-conjugation and microstructural ordering. A similar trend is observed in oligothiophenes.[50]

For compound **10**, the thin-film optical absorption spectrum changes significantly on annealing. Solution-cast films exhibit two absorption maxima at 313 and 387 nm, and upon annealing at 120 °C, the absorption maxima red-shift to 340 and 412 nm ($\Delta\lambda_{max} \approx 25$ nm), respectively, and two new features at longer wavelengths (688 and 759 nm) appear. The intensity of the two new peaks and the absorption maximum at 412 nm increases upon annealing at 150 °C, suggesting a high degree of macromolecular organization in the thin-film phase and enhancement of the molecular packing which is further confirmed by thin-film XRD and AFM analyses (vide infra).

The solution PL emission spectra of compounds **1**−**12** are shown in Figure 6 and data are collected in Table 1. Since 0−0 transitions are rarely observed in room temperature solution spectra, it is an accepted procedure to use $\Delta = \lambda_{em} - \lambda_{abs}$ as an estimation of the magnitude of the Stokes shift.[51] When carbonyl functionalized compounds **1**, **3**, **5**, **7**, **9**, and **11** are excited at short-wavelength absorption maxima, emissions are observed at 540−675 nm, indicating large Stokes shifts of ~150−390 nm. These large Stokes shifts, which are surprising considering the planar backbones of the present ladder-type cores, have also been observed in the literature for carbonyl-functionalized pentaphenylene compounds.[52] Such large Stokes shifts are attributed to the fact that when two chromophore units are in conjugation (i.e., bis(indenofluorene) and carbonyl/dicyanovinylene) intramolecular energy transfer between the excited states of two chromophore units ($T_{\pi-\pi^*}/S_{\pi-\pi^*}$ and $T_{n-\pi^*}/S_{n-\pi^*}$) occurs until the lowest excited-state is reached, resulting in large Stokes shifts.[52] Interestingly, excitation of the present compounds at their long-wavelength absorption maxima yields emissions identical to those of short-wavelength absorption maxima. This suggests similarities of the emission pathways and final relaxed excited states of these molecules upon either $\pi-\pi^*$ or $n-\pi^*$ excitation. This similarity in emission characteristics further confirms the presence of highly efficient intramolecular energy transfer between chromophore units ($S_{1(\pi-\pi^*)} \rightarrow S_{1(n-\pi^*)}$). The fluorescence spectra of the carbonyl compounds exhibit positive solvachromatisms, ($\Delta\lambda = 40-60$ nm for cyclohexane ($\varepsilon = 2.0$) → THF ($\varepsilon = 7.6$) → ethanol ($\varepsilon = 30.0$)), even larger than that observed in the long-wavelength absorption maxima, indicating that the dipole moment is larger in the excited state than in the ground state and the final relaxed excited state has some charge transfer (CT) characteristics (Figure 7). When the electron-deficiency of the core increases with dicyanovinylene functionalization, the Stokes shift increases and only very weak, broad peaks are observed at 760−785 nm for dicyanovinylene-functionalized compounds **2**, **4**, **6**, **8**, **10**, and **12**. This is consistent with the general observation that increased Stokes shift amplitudes generally correlate with longer excited-state lifetimes, resulting in an increase in the relative probability of nonradiative decay and lower PL quantum efficiencies.[53] This suggests that the core electron-deficiency operates via intramolecular energy-/charge-transfers which result in large Stokes shifts and eventual quenching.[54] To investigate the importance of charge-transfer excited states in these dicyanovinylene compounds, fluorescence spectra were recorded in cyclohexane,

(44) Ferraris, J. P.; Lambert, T. L. *J. Chem. Soc., Chem. Commun.* **1991**, 1268–1270.
(45) Merlet, S.; Birau, M.; Wang, Z. Y. *Org. Lett.* **2002**, *4*, 2157–2159.
(46) Facchetti, A.; Letizia, J.; Yoon, M.-H.; Mushrush, M.; Katz, H. E.; Marks, T. J. *Chem. Mater.* **2004**, *16*, 4715–4727.
(47) Yassar, A.; Horowitz, G.; Valat, P.; Wintgens, V.; Hmyene, M.; Deloffre, F.; Srivastava, P.; Lang, P.; Garnier, F. *J. Phys. Chem.* **1995**, *99*, 9155–9159.
(48) Facchetti, A.; Yoon, M. H.; Stern, C. L.; Hutchison, G. R.; Ratner, M. A.; Marks, T. J. *J. Am. Chem. Soc.* **2004**, *126*, 13480–13501.
(49) Pan, H.; Wu, Y.; Li, Y.; Liu, P.; Ong, B. S.; Zhu, S.; Xu, G. *Adv. Funct. Mater.* **2007**, *17*, 3574–3579.
(50) Meng, H.; Zheng, J.; Lovinger, A. J.; Wang, B.-C.; Van Patten, P. G.; Bao, Z. *Chem. Mater.* **2003**, *15*, 1778–1787.
(51) Pope, M.; Swenberg, C. E. *Electronic Processes in Organic Crystals*; Oxford University Press: New York, 1982.
(52) Jacob, J.; Sax, S.; Piok, T.; List, E. J. W.; Grimsdale, A. C.; Müllen, K. *J. Am. Chem. Soc.* **2004**, *126*, 6987–6995.
(53) Berlaman, I. B. *Fluorescence Spectra of Aromatic Molecules*; Academic Press: New York, 1971.
(54) Turro, N. J. *Modern Molecular Photochemistry*; University Science Books: Sausalito, CA, 1991.

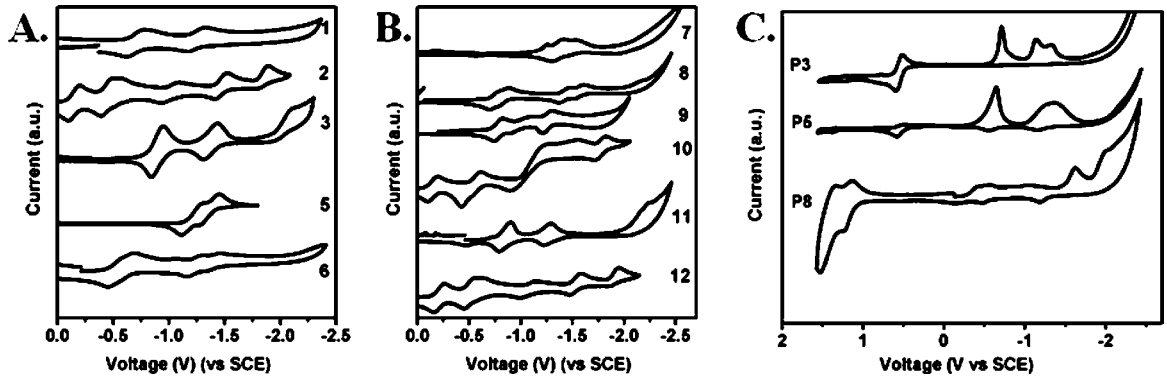

Figure 8. Cyclic voltammograms of molecules **1**−**12** as solutions in THF (A and B) and representative polymers **P3**, **P5**, and **P8** as thin films in acetonitrile (C) in 0.1 M $Bu_4N^+PF_6^-$ at scan rates of 100 mV/s.

and broad, significantly blue-shifted fluorescence peaks at 460−500 nm were observed which are absent in THF (Figure 7). This indicates the formation of a charge-transfer excited-state in relatively polar THF, resulting in fluorescence quenching. The formation of charge-transfer states for these dicyanovinylene-based compounds may be especially favorable due to arene and cyano group resonance stabilization of the corresponding cations and anions. The dicyanovinylene-functionalized compounds exhibit significant bathochromic shifts of ∼115−240 nm in the emission maxima versus those of the carbonyl-functionalized analogues, and furthermore, upon introduction of thiophene units, emission red-shifts of ∼5−50 nm are observed for **3**, **4**, **7**, **8**, **11**, and **12**, consistent with the optical absorption. Thin-film fluorescence spectra were obtained by excitation at $\lambda_{abs}^{thin\text{-}film}$, and data are summarized in Table 1. In general, the trends from solution are preserved in the thin films. The spectral shapes and maxima are similar to the solution spectra with additional peaks for compounds **1** and **3**. Thin films of the dicyanovinylene-functionalized compounds exhibit very broad, weak peaks, consistent with the solution phase results.

In THF, polymers **P2**, **P3**, **P4**, **P6**, **P7**, **P8**, **P12**, **P13**, and **P14** exhibit absorption maxima at 460, 401, 465, 418, 426, 456, 420, 461, and 460 nm, respectively, with shoulders on the red side of the bands at 600, 497, 680, 577, 514, 661, 560, 810, and 808 nm, respectively. All of these polymers show bathochromic shifts of ∼20−60 nm compared to their monomeric counterparts (**2**, **3**, **4**, **6**, **7**, **8**, **9**, and **10**) as expected due to the extended π-conjugation. The thin-film absorption maxima are observed at 455, 393, 457, 405, 421, 435, and 471 nm for **P2**, **P3**, **P4**, **P6**, **P7**, **P8**, **P12**, **P13**, and **P14**, respectively, with shoulders at 620, 485, 705, 587, 512, 709, 605, 847, and 845 nm, respectively. Band gaps are estimated to be 1.55 eV for **P2**, 1.70 eV for **P3**, 1.45 eV for **P4**, 1.99 eV for **P6**, 2.06 eV **P7**, 1.57 eV for **P8**, 1.90 eV for **P12**, 1.38 eV for **P13**, and 1.37 eV for **P14** from the low-energy absorption edges. In general, introduction of thiophene units into the polymer backbone results in red-shifts of the absorption maxima and contraction of the band gaps, reflecting the combined effects of π-electron-donating S atoms vs the C=C linkages, the presence of donor/acceptor backbones, and the more planar conformation of five−five vs five−six inter-ring linkages.[55]

Electrochemical Characterization. The electrochemical properties of the present compounds **1**−**12** and polymers **P1**−**P13** were characterized by cyclic voltammetry in solution and as thin films. Cyclic voltammograms are shown in Figure 8, and electrochemical data are summarized in Tables 1 and 2. The ferrocene/ferrocenium couple was used as an internal standard, and all potentials are reported vs SCE. Analysis of the half-wave potentials provides substantial information on the effects of carbonyl/dicyanovinylene functionalization, relative π-core size, and thiophene content in modulating the frontier MOs.

In THF, all ladder-type compounds exhibit multiple reversible reductions with the first half-wave potentials ranging from −1.20 to −0.12 V. The completely reversible reductions at low potential magnitudes reveal the marked electron-deficiency of these new core structures and their potential electron-transporting nature with stable doping/dedoping characteristics. Indenofluorene compounds **1**, **2**, **3**, and **4** exhibit multiple reversible reductions with first half-wave potentials of −0.77, −0.14, −0.90, and −0.24 V, respectively (vs SCE). The first half-wave reduction potentials for bisindenofluorene-based compounds **5**, **6**, **7**, and **8** are −1.20, −0.53, −1.25, and −0.72 V, respectively (vs SCE), which are ∼0.4−0.5 V lower than those of the indenofluorene compounds having similar electron-withdrawing functionalities, suggesting lower electron affinities due to relatively large core-sizes. Indenofluorene-based compounds **9**, **10**, **11**, and **12** having thiophenes at the molecular termini also exhibit multiple reduction events with the first half-wave potentials at −0.74, −0.12, −0.85, and −0.20 V, respectively. Ladder-type diketone cores **1** and **5** can be reduced far more easily than the corresponding nonladder terphenylene and quaterphenylene compounds which show reversible reductions at −2.40 and −2.28 V (vs SCE), respectively.[56] Clearly, reduction potentials are shifted to more positive values with increasing degree of planarity and core electron deficiency, consistent with the initial design considerations (vide supra).

From the first half-wave reduction potentials, LUMO energies ($EA^{red} \approx -LUMO^{red}$ assuming that Koopmans' theorem holds) for the present compounds can be estimated by taking the SCE energy level to be −4.44 eV below the vacuum level and using the relation of eq 3.[11,57]

$$LUMO^{red} = -E_{red\text{-}1/2} - 4.44 \quad (3)$$

Results are summarized in Table 1. Using this relationship, solution-phase $LUMO^{red}$ values are estimated to lie at −3.67, −4.30, −3.54, −4.20, −3.70, −4.32, −3.59, and −4.20 eV for

(55) Lu, G.; Usta, H.; Risko, C.; Wang, L.; Facchetti, A.; Ratner, M. A.; Marks, T. J. *J. Am. Chem. Soc.* **2008**, *130*, 7670–7685.
(56) Meerholz, K.; Heinze, J. *Electrochim. Acta* **1996**, *41*, 1839–1854.
(57) Zhu, Y.; Champion, R. D.; Jenekhe, S. A. *Macromolecules* **2006**, *39*, 8712–8719.

indenofluorene-based compounds **1**, **2**, **3**, **4**, **9**, **10**, **11**, and **12**, respectively. The $LUMO^{red}$ energies for bisindenofluorene-based compounds **5**, **6**, **7**, and **8** are estimated to be −3.24, −3.91, −3.19, and −3.72 eV, respectively. The low LUMO energies (≤ −3.2 eV) for all of the present ladder-type compounds suggest that these materials have high electron affinities and are good candidates for n-channel semiconductors. The LUMOs for **2**, **4**, **10**, and **12** are therefore within the range of those of the aforementioned air-stable arylenediimide semiconductors PDI-8CN2, ADI-8CN2, and NDI-8CN2 with $LUMO^{red} < -4.0$ eV.[15,16,18]

For (bis)indenofluorene compounds **1**, **2**, **5**, **6**, and **9**, dicyanovinylene functionalization anodically displaces the first half-wave potentials by ∼0.6 V suggesting that the highly electron-withdrawing dicyanovinylene substituents dramatically affect the LUMO energies, and in similar ways for all compounds. In marked contrast, the corresponding displacements in HOMO energies are much smaller ($\Delta \approx +0.20$ eV), suggesting that the LUMOs are primarily localized on the bridge methylenes, which renders them more susceptible to functionalization, whereas the HOMOs are more delocalized over the entire molecule, consistent with the DFT results (vide infra). Dicyanovinylene functionalization in both indenofluorene and bisindenofluorene cores reduces the voltage spacing between the first two reductions by 0.1−0.2 V and increases the number of observed reductions, reflecting the more electron-accepting nature of these derivatives and the greater number of possible reduction sites. This similarity in the first two potentials suggests that the greater facility of the second reduction is due to the enhanced electron-deficiency of the core, and that these reductions are largely malononitrile-centered, as previously observed for tricyanovinyl-capped oligothiophenes.[58,59]

Relative core size effects on the stabilization of subsequent reductions is observed for (bis)indenofluorene compounds **1**−**8**. For compound pairs **1** and **5**, **2** and **6**, **3** and **7**, and **4** and **8**, having similar functionalities, the potential difference between successive reduction events [$\Delta E_{1/2} = E_{1/2-2} - E_{1/2-1}$] are, without exception, smaller for the bisindenofluorene cores by ∼0.3 V versus the indenofluorene cores. This trend is attributed to more effective radical anion delocalization and decreased Coulombic repulsions within the larger bisindenofluorene π-system.[51,60] A similar trend is observed in the α-nT and phenylene (p-nP) semiconductor series.[61]

Addition of thiophene substituents to the electron-deficient bis(indenofluorene) compounds **1**, **2**, **5**, **6**, **9**, and **10** results in an increase in HOMO energies by ∼0.2−0.4 eV, reflecting the π-electron-rich thiophene nature versus the electron-deficient cores. Due to the increased effective π-conjugation lengths of the molecules, the LUMO energies exhibit smaller displacements of ∼0.1−0.2 eV, and eventually the band gaps contract ($\Delta E_g = 0.1-0.3$ eV), consistent with the optical data discussed above. The DFT-derived orbital contours also show that the thiophene units make greater contributions to the HOMOs than the LUMOs, which explains the observed energy shifts upon thiophene addition. It will be seen below that the large observed positive HOMO shifts along with the smaller LUMO changes provide three new molecules **3**, **9**, and **12**, which are ambipolar semiconductors having both electron and hole injection accessible MOs.

Thin-film electrochemical data for the present compounds follow the general trends of the solution phase data, indicating similar molecular structure effects on the solution and solid-state electrochemical properties. Similar reduction values ($\Delta E_{1/2-1} < 0.1-0.2$ V) are observed along with more evident oxidation peaks ($E_{onset-1} = +1.10$ to $+1.40$ V). Electrochemical band gaps estimated from reduction and oxidation potentials ($E_g^{CV} = 1.50-2.36$ eV) exhibit parallel trends to those observed in solution/thin-film optical band gaps, supporting the accuracy of the two different techniques used to analyze electronic structure.

Cyclic voltammetric data for the present polymers were measured as thin films on Pt working electrodes in acetonitrile. Representative voltammograms are shown in Figure 8, and data are summarized in Table 2. The onset of reduction and oxidation potentials are −0.12 and 1.37 V, −0.80 and 0.98 V, −0.29 and 1.12 V, −0.37 and 1.31 V, −0.90 and 0.90 V, −0.60 and 1.12 V, −0.82 and 0.98 V, −0.29 and 1.07 V, and −0.27 and 1.10 V for polymers **P2**, **P3**, **P4**, **P6**, **P7**, **P8**, **P12**, **P13**, and **P14**, respectively. Using eq 1, the LUMO/HOMO energies are calculated as −4.32/−5.81 eV for **P2**, −3.64/−5.42 eV for **P3**, −4.15/−5.56 eV for **P4**, −4.07/−5.75 eV for **P6**, −3.54/−5.34 eV for **P7**, −3.84/−5.56 eV for **P8**, −3.62/−5.42 eV for **P12**, −4.15/−5.51 eV for **P13**, and −4.17/−5.54 eV for **P14**. Without exception, thiophene addition to the electron-deficient core structures increases both the HOMO and LUMO energies with a larger increase in the former and results in band gap contractions. The polymer electrochemical features strongly reflect the nature of the individual building blocks, indicating that polymer electronic properties are determined principally by the backbone chemical structure with negligible contributions from molecular weight differences. For **P13** and **P14**, the exceptionally low LUMO energies (−4.15 to −4.17 eV) with low band gaps (1.36−1.37 eV) render these polymers attractive as potential ambipolar semiconductors capable of exhibiting air-stable electron and hole transport, a phenomena yet to be observed.

Single-Crystal Structures. Single crystals of the new compounds **7**, **M2**, and **M4** were grown by slow diffusion of methanol into chloroform solutions (for **7** and **M2**) and slow evaporation of chloroform solutions (for **M4**), respectively, and the crystal structures determined by X-ray diffraction are shown in Figure 9. The conjugated backbone of thiophene-terminated bisindenofluorenedione compound **7** adopts a substantially planar molecular configuration with very small plane-to-plane twist angles of 1.3° and 1.2° between the outer phenyl rings 1 and 2, and 3 and 4, respectively. The twist angle is 1.4° between the innermost two phenyl rings, 2 and 3. One of the outer thiophene rings lies within the plane of the ladder core with small twist angle of 0.6°, whereas the other thiophene unit exhibits a larger twist angle of 7.3°, which is comparable to those observed in planar alkyl and perfluoroalkyl substituted oligothiophenes (∼5−6°).[46,48] The thiophene rings at the molecular termini display a typical trans conformation. In addition, the carbonyl groups are effectively in conjugation with the conjugated backbone since they are within 2° of the molecular plane. In spite of the highly planar backbone of **7**, no evidence of extended π−π stacking interactions is observed, and it is seen that packing is mainly governed by van der Waals interactions between linear alkyl-chains (n-$C_{12}H_{25}$) forming

(58) Bader, M. M.; Custelcean, R.; Ward, M. D. *Chem. Mater.* **2003**, *15*, 616–618.
(59) Pappenfus, T. D.; Burand, M. W.; Janzen, D. E.; Mann, K. R. *Org. Lett.* **2003**, *5*, 1535–1538.
(60) Yoon, M.-H.; Facchetti, A.; Stern, C. E.; Marks, T. J. *J. Am. Chem. Soc.* **2006**, *128*, 5792–5801.
(61) Meerholz, K.; Heinze, J. *Electrochim. Acta* **1996**, *41*, 1839–1854.

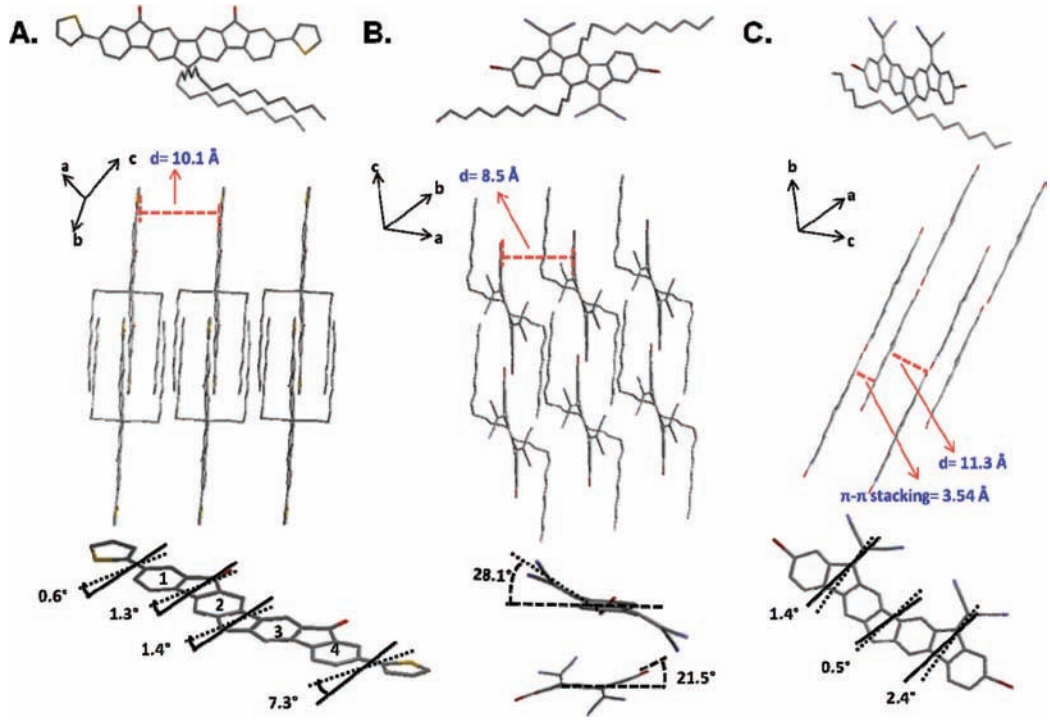

Figure 9. Single-crystal X-ray structures of (A) bisindenofluorenediketone compound **7**, (B) indenofluorenedicyanovinylene monomer **M2**, and (C) bisindenofluorenedicyanovinylene compound **M4**.

alternating layers of insulating alkyl chains and conductive π-conjugated backbones. The conjugated backbones of **7** orient perfectly in a face-to-face manner, and the alkyl chains exhibit substantial interdigitation with greater than ~10 methylene ($-CH_2-$) units directing the self-assembly process. The minimum distance between the closest arene rings is ~10.1 Å. The molecular length is measured as 24.4 Å along the conjugated backbone. To the best of our knowledge, the tetraphenylenediketone core is one of the longest ladder-type *p*-phenylene oligomers to date that has been characterized by X-ray diffraction.

In contrast to the planar backbone of **7**, the central arene ring of compound **M2** exhibits torsion angles up to 9.1°, resulting in a "wavey" structure. The outer arene rings are twisted ca. 21.5° out of the plane of the central arene core, which approaches the ~30° maximum value beyond which there is insufficient intramolecular π-overlap to support a significant π-conjugated structure.[48] As shown in Figure 9, the dicyanovinylene functionalities are displaced ca. 28.1° out of the cyclopentadienyl planes, indicating significantly reduced conjugation between these electron-deficient functionalities and the π-conjugated core. The observed, highly twisted **M2** backbone is largely a result of the steric hindarence between the alkyl chains at positions 5 and 11, and the dicyanovinylene groups at positions 6 and 12. Similar to the packing motif in **7**, van der Waals interactions between alkyl chains (over 10 methylene units ($-CH_2-$)) primarily direct the crystal packing, resulting in segregated layers of alky chains and π-conjugated backbones. The minimum distance between the closest arene rings is measured as ~8.5 Å.

Dicyanovinylene-functionalized bisindenofluorene compound **M4** adopts a highly planar molecular backbone with small plane-to-plane twist angles of 2.4°, 1.4°, and 0.5° between the outer arene rings and innermost two arene rings, respectively. In contrast to **M2**, the dicyanovinylene functionalities lie completely within the cyclopentadienyl plane, indicative of a high degree of conjugation between these functionalities and the π-conjugated core. The molecules are π-stacked in a slipped cofacial orientation along the long axis of the molecule at an interplanar $\pi-\pi$ stacking distance of 3.54 Å. The existence of the $\pi-\pi$ stacking interactions in **M4** explains the relatively high melting point in the solid state versus those of **7** and **M2** which do not exhibit $\pi-\pi$ stacking. The molecular length is measured as 18.9 Å, and the molecular backbones of adjacent molecules exhibit $\pi-\pi$ stacking interactions over 8.7−8.8 Å lengths along the molecular axes.

The observed alkyl chain interaction-dominated crystal structures of **7** and **M2** explain the observed, relatively low melting points (T_m < 170 °C) compared to previously reported oligothiophenes and other dicyanovinylene-functionalized compounds of the present new family (**6**, **8**, and **10**), which exhibit much stronger $\pi-\pi$ interactions. Despite the lack of $\pi-\pi$ interactions in the single crystal structures, the molecules exhibit highly ordered $\pi-\pi$ stacked lamella structures in the thin-film phase (vide infra).

Thin-Film Morphology. Thin-film microstructures, morphologies, and molecular orientations for the present new class of materials were studied by $\theta-2\theta$ X-ray diffraction (XRD), grazing incidence X-ray diffraction (GIXRD), and AFM. Additionally, XRD rocking curves were recorded to evaluate out-of-plane film texturing. Since direct in situ characterization of microstructure at the burried dielectric−semiconductor interface, the active region for charge transport,[62] is not possible with conventional techniques, we studied the morphology of the semiconductor surface and crystallinity across the entire film, with the reasonable assumption that they resemble the basic microstructure at the interface. This approach has been previously successful in elucidating thin film feature−device per-

(62) Horowitz, G. *J. Mater. Res.* **2004**, *19*, 1946–1962.

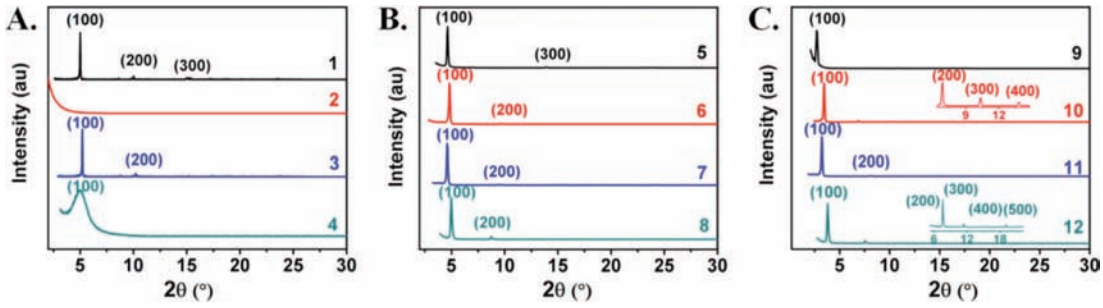

Figure 10. $\theta-2\theta$ X-ray diffraction (XRD) scans of spin-cast films of compounds **1**−**12** on silicon substrates.

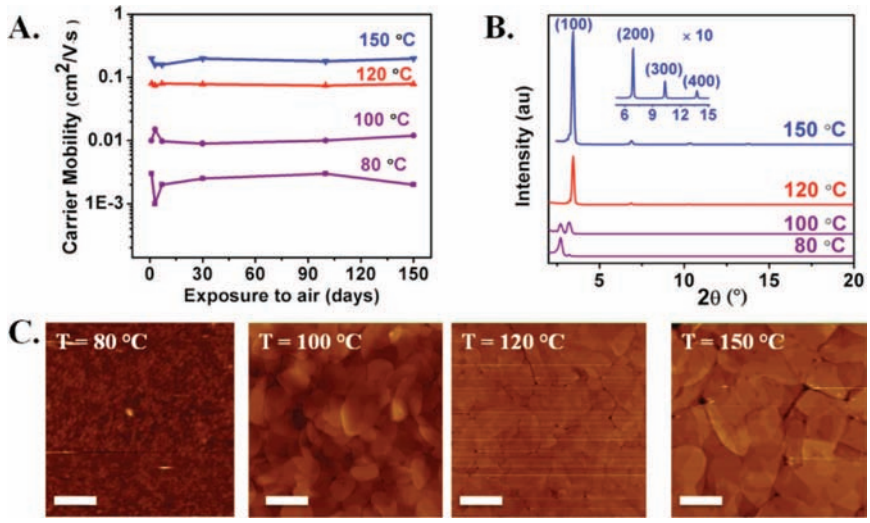

Figure 11. (A) Electron mobilities measured in ambient for TFTs fabricated with spin-coated **10** and annealed at the indicated temperatures (80−150 °C) vs storage time of the devices in air without excluding light or ambient humidity (25−40%). (B) $\theta-2\theta$ X-ray diffraction (XRD) scans of spin-coated **10** thin films after annealing at the indicated temperatures (Note that peak intensities are not normalized for comparative purposes). (C) Tapping mode AFM images of **10** thin films after annealing at the indicated temperatures. Scale bars denote 1 μm.

Table 4. XRD Reflections and *d*-Spacings Calculated from the (100) Reflection for Vacuum-Deposited and Solution-Cast Films of Compounds **1**−**12**

		2θ (*d*-spacing (Å)) (°)	
compd	reflections	vacuum	solution
1	(100), (200), (300)	4.80 (18.4)	4.99 (17.7)
2	–	–	–
3	(100), (200)	5.10 (17.3)	5.16 (17.1)
4	(100)	5.15 (17.1)	5.00 (17.6)
5	(100), (300)	4.55 (19.4)	4.65 (18.9)
6	(100), (200)	4.74(18.4)	4.85 (18.2)
7	(100), (200)	4.55 (19.4)	4.60 (19.2)
8	(100), (200)	4.80 (18.4)	4.99 (17.7)
9	(100), (200)	2.75 (32.1)	2.70 (32.7)
10	(100), (200), (300), (400)	3.40 (25.9)	3.43 (25.7)
11	(100), (200)	–	3.20(27.6)
12	(100), (200), (300), (400), (500)	–	3.80 (23.2)

formance relationships for a variety of thiophene-, arylene-, and acene-based semiconductors.[13,19,55] Measurements were carried out on vacuum-deposited and spin-coated thin films grown on OTS-treated Si/SiO_2 substrates. The thicknesses of all films were 50−60 nm by profilometry. The XRD scans reveal that films of compounds **1**, **3**, and **4**−**12**, prepared by vacuum deposition or solution-casting, are highly textured. Representative XRD scans and AFM images of solution-cast films are shown in Figures 10 and 11, respectively, and data are collected in Table 4.

Out-of-plane $\theta-2\theta$ XRD scans exhibit several sharp low-angle reflections with high intensities up to fifth order, revealing that vacuum-deposited films are highly ordered. However, in general, the solution-deposited films exhibit lower degrees of crystalline order compared to the vacuum-deposited films, which can be explained by the relatively high rate of the film growth using this method (T_D < 1 min) for solution-cast films, resulting in relatively less-ordered microstructures versus the vacuum-deposited films (T_D > 1 h).[21] The only exception is the thin films of **10** which exhibit very high degrees of crystallinity from solution, similar to the vacuum-deposited films, and indicating very favorable molecular ordering for this particular donor−acceptor compound from solution. For all films, a single family of diffraction peaks are observed without the presence of an obvious $\pi-\pi$ stacking feature, and *d*-spacing values are estimated from the (100) diffraction peaks as 17.1−32.7 Å, implicating a crystalline polymorph where the majority of the molecules have an edge-on orientation on the substrate with the $\pi-\pi$ stacking direction parallel to the substrate, thereby favoring in-plane charge transport from source to drain. From the GIXRD measurements, $\pi-\pi$ stacking distances are estimated as 3.1−3.7 Å, which is in the range of distances measured for many oligo-/polythiophene and fluorene-based semiconductors.[1,55,63] Note that exceptionally short stacking distances of 3.1 Å are observed for thin films of **10**, **P13**, and **P14**, indicating

(63) Murphy, A. R.; Liu, J. S.; Luscombe, C.; Kavulak, D.; Frechet, J. M. J.; Kline, R. J.; McGehee, M. D. *Chem. Mater.* **2005**, *17*, 4892–4899.

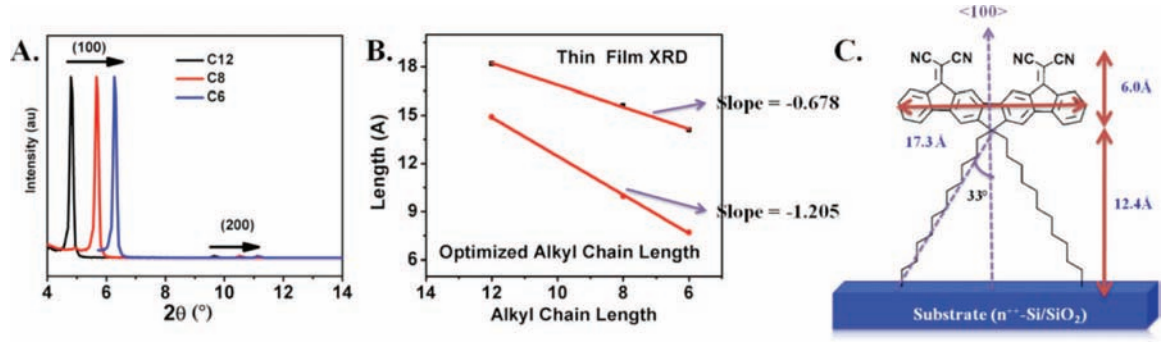

Figure 12. (A) $\theta-2\theta$ X-ray diffraction (XRD) scans of spin-cast films of compound **6** with *n*-hexyl, *n*-octyl, and *n*-dodecyl substituents on silicon substrates. (B) Experimental *d*-spacings and theoretical alkyl chain lengths versus the number of carbon atoms in the substituent. (C) Proposed molecular structure in the thin film phase (<100> is arbitrarily defined as perpendicular to the substrate plane).

geometrically favorable $\pi-\pi$ interactions between molecular backbones. Rocking curves of the first-order reflections (100) for all samples indicate a high degree of texturing (fwhm = 0.03−0.04°, corresponding to the resolution of the instrument), demonstrating that the film microstructure layers are uniformly oriented relative to the substrate plane. Compounds **2** and **4** have significantly poor crystallinities in the thin film phase, probably due to their nonplanar backbones and out-of-plane distorted dicyanovinylene functionalities, as evidenced from the single-crystal X-ray structures, which reduces efficient $\pi-\pi$ stacking interactions. As expected from the highly planar core structures observed in **7** and **M4** by single-crystal diffraction, bisindenofluorene-based compounds **6**−**8** form highly crystalline thin films, presumably a result of efficient $\pi-\pi$ stacking interactions between planar backbones. Simulated powder patterns for the present single-crystal structures reveal correlations with the reflections in thin-film XRD data, suggesting that these compounds adopt somewhat different packing as thin films. Due to the presence of alkyl-chain interdigitation, estimation of molecular tilt angles from *d*-spacings and estimated molecular lengths is not straightforward as in the case of oligothiophene- and acene-based semiconductors.[13] For indenofluorene-based compounds **1**−**4** and **9**−**12**, in which the *n*-dodecyl chains protrude directly from the thiophene or arene units, the molecular backbone tilt-angles relative to the substrate are highly dependent on the degree of alkyl-chain interdigitation. For bisindenofluroene-based compounds **5**−**8**, in which alkyl chains protrude from the bridge methylene, molecular orientation was studied as a function of the alkyl substituent length. Thin films of **6** were fabricated from the *n*-hexyl (C_6H_{13}), *n*-octyl (C_8H_{17}), and *n*-dodecyl ($C_{12}H_{25}$) substituted derivatives under exactly the same conditions to compare out-of plane crystallinity. Although crystallinities are qualitatively similar, judging from XRD intensities, fwhm, and numbers of visible reflections, the *d*-spacing value progressively falls when the substitutients are changed from *n*-dodecyl to *n*-octyl to *n*-hexyl chains (18.4 → 15.6 → 14.1 Å), corresponding to a change of 0.68 Å per carbon atom. This difference corresponds to the difference in the distance from the end of the alkyl groups to the edge carbon atoms of the central fluorene core obtained by DFT calculations (∼1.21 Å per atom), suggesting that the alkyl chains are oriented along the substrate surface normal with tilt angles of ∼33°, and that the molecular backbone is nearly perpendicular to the substrate (Figure 12).

The degrees of crystallinity of solution-cast films of **10** are highly dependent on the annealing temperature. As shown in Figure 11, a change in the preferential crystalline phase/orientation is observed upon annealing, with the *d*-spacing decreasing from 32.7 to 25.7 Å and with a significant increase in the (100) reflection intensity (5000 → 65 000 count/s), and higher order reflections (200, 300, and 400) become evident, indicative of higher degree of ordering, enhanced alkyl-chain interdigitation (Δ > 7 methylene ($-CH_2-$) units), and/or molecular tilting from the substrate normal. This crystalline phase transition occurs at 80−100 °C, corresponding to the thermal transition observed at 93 °C by DSC (vide supra). AFM analysis shows that upon annealing, the morphology changes from ball-like grains with sizes of <0.1 μm to very large ∼3−5 μm platelike grains of terraced islands with step heights of ∼2.8 nm, corresponding to the observed lamellar XRD *d*-spacing. The large polycrystalline grains of **10** are unlike any film reported for a solution-cast n-channel semiconductor to date, and are significantly larger than the length scale of lithographically accessible channel lengths (∼100 nm), offering the possibility of fabricating grain boundary-free, single-crystal-like transistors from straightforwardly solution-processed thin films. A similar crystalline phase transformation is observed for the polymers **P13** and **P14**; however, it is not associated with an increase in the grain size, indicating that ordering occurs only within the grain, without facilitating connectivity and ordering between grains. Importantly, we observe that these two different types of crystallinity increases for **P13**/**P14** versus **10** have totally different impacts on the final OTFT device performances (vide infra). On the basis of the aforementioned GIXRD, out-of-plane XRD, and AFM results at different film annealing temperatures, the molecular plane of **10** is estimated to be nearly perpendicular to the substrate ($\theta \approx 90°$) and the alkyl chains are interdigitated over >7 methylene ($-CH_2-$) units, consistent with the single-crystal structural features. A schematic figure showing the proposed $\pi-\pi$ stacked thin-film microstructure of **10** is shown in Figure 13.

Thin-Film Transistor Device Characterization. OTFTs with top-contact/bottom gate device structures were fabricated by either vacuum deposition or spin-coating on OTS-treated SiO_2/p^+-Si substrates. All spin-coating processes were carried out in ambient, and devices were then annealed at 80−150 °C for 30 min under nitrogen. Vapor phase depositions were carried out under high vacuum (1×10^{-6} Torr) with the substrates maintained at temperatures (T_D) of 70 or 110 °C. Finally, gold contacts were patterned by thermal evaporation using shadow masks to give channel lengths of 25−100 μm and widths of 500−2000 μm. FET properties were evaluated under positive or negative gate bias in ambient/vacuum to explore the majority charge carrier type, device performance, and enviromental stability. All electron/hole mobilities and threshold voltages are calculated in the saturation regime. FET data are summarized

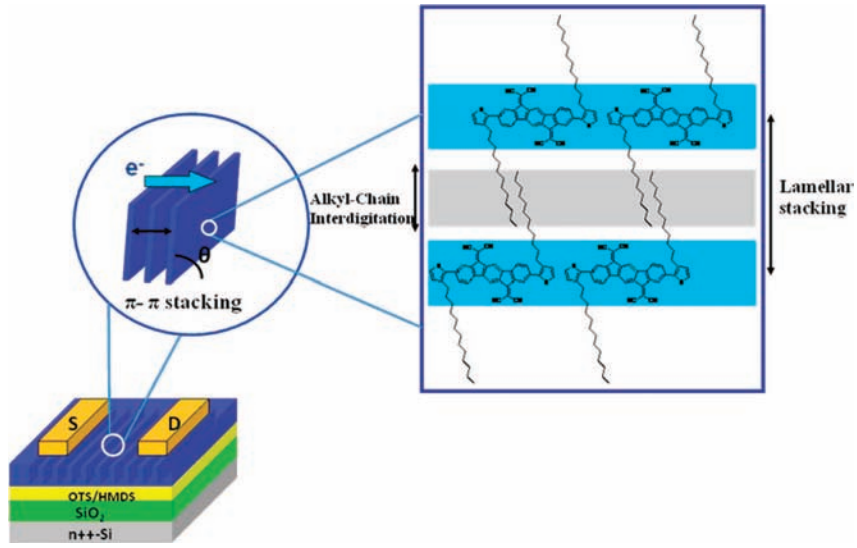

Figure 13. Schematic model of the $\pi-\pi$ stacked thin-film microstructure of compound **10**. The gray region shows the interdigitated alkyl chains forming an insulating barrier between the conducting π-conjugated backbones (blue region). Note that the tilt angle (θ) strongly depends on the extent of alkyl-chain interdigitation for a given *d*-spacing.

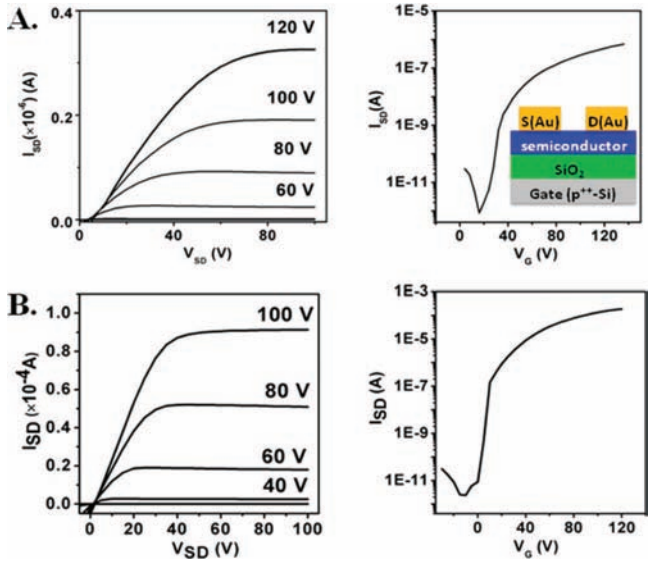

Figure 14. OTFT data for devices fabricated with compounds **6** and **10**. (A) Output and transfer ($V_{SD} = 100$ V) plots for films of **6**. (B) Output and transfer ($V_{SD} = 100$ V) plots for films of **10**. The general structure of an OTFT device is given in the inset.

in Tables 2 and 3, and representative transfer and output plots are shown in Figure 14.

Devices fabricated with compounds **1**, **2**, and **5** are found to exhibit no FET activity, whereas compounds **3**, **4**, and **6**−**12** exhibit FET activity as p-channel, n-channel, or ambipolar semiconductors. It is found that compounds **7** and **11** are p-channel semiconductors with air-stable hole mobilites up to 0.001 and 1×10^{-4} cm^2/V·s, respectively. Compounds **3**, **9**, and **12** exhibit ambipolar behavior with appreciable electron mobilities up to 0.01 cm^2/V·s and hole mobilities up to 0.006 cm^2/V·s. Although compounds **3** and **9** operate only under vacuum, similar to most reported ambipolar semiconductors in the literature,[64] FETs fabricated with **12** are found to operate in ambient. To the best of our knowledge, this is the first example of a thiophene-based molecular semiconductor showing air-stable charge transport of both holes and electrons.[1,64] Additionally, FETs based on **9** exhibit highly balanced electron and hole mobilities of 0.006 cm^2/V·s ($\mu_e/\mu_h \approx 1.0$) for the vacuum-deposited films ($T_D = 110$ °C) which indicates that the solid-state microstructure and MO energetics facilitate both hole and electron transport with similar efficiency.[13]

OTFTs fabricated with dicyanovinylene-functionalized compounds **4**, **6**, **8**, and **10** exhibit n-channel behavior with electron mobilities and I_{on}/I_{off} ratios of 0.001 cm^2/V·s and 10^5 (**4**), 0.006 cm^2/V·s and 10^6 (**6**), 0.02 cm^2/V·s and 10^6 (**8**), and 0.16 cm^2/V·s and 10^7 (**10**). Devices of **6** and **8** are adversely affected by ambient conditions and operate only under vacuum. However, highly electron-deficient (low-energy LUMO) compounds **4** and **10** exhibit stable n-channel activities in air, a significant advance over many reported n-channel semiconducting materials.[6] Devices stored under ambient without excluding light or humidity exhibit very stable device performance over time, and similar electron mobilities and I_{on}/I_{off} ratios are measured after 5 months of storage in air (Figure 15).

Solution-cast thin films (50−65 nm) were fabricated by spin-coating 5 mg/mL solutions of the semiconductors in air, and devices were then annealed at 80−150 °C under N_2 for 30 min. Although the polymeric semiconductors are found to form smooth thin films from any solvent, molecular semiconductors tend to form continuous thin films only from low-boiling-point solvents (e.g., $CHCl_3$, THF). This may be due to the high volatility of the solvent which facilitates rapid, smooth film growth on the highly hydrophobic OTS surface (advancing aqueous contact angle = 110−120°) before being spread during the spin-coating process.[55] Charge carrier transport type and ambient stability trends follow those of the vacuum-deposited films, although in general one to 2 orders of magnitude lower mobilities (1×10^{-4}−0.16 cm^2/V·s) are measured for the solution-cast devices. This depressed performance principally reflects the low degree of microstructural order achieved in solution-cast films as evidenced by the XRD and AFM data. Surprisingly, although vacuum-deposited devices of **3** exhibit ambipolar behavior, solution-cast devices exhibit only p-channel activity ($\mu_h = 0.001$ cm^2/V·s, $I_{on}/I_{off} = 10^5$), suggesting that

(64) Zaumseil, J.; Sirringhaus, H. *Chem. Rev.* **2007**, *107*, 1296–1323.

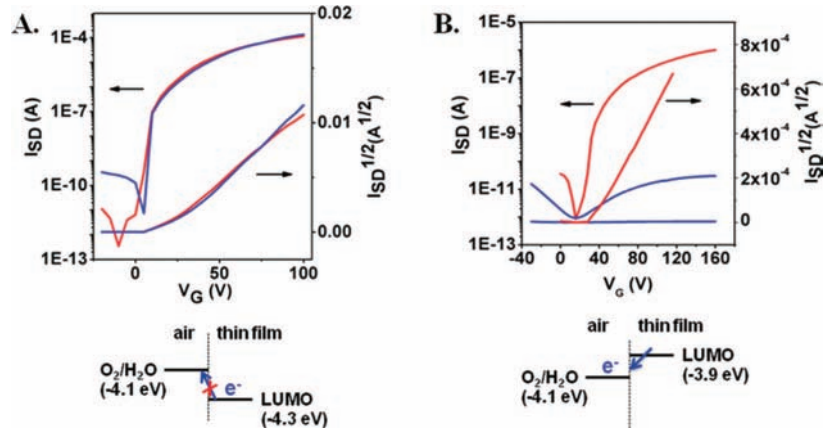

Figure 15. Transfer curves of compounds **10** (A) and **6** (B) under vacuum (red curves) and in ambient (blue curves). Note that the transfer curve for compound **10** was recorded after 5 months of storage in ambient. Below: the band lineups of LUMO energies of **6** and **10** with respect to the O_2/H_2O electrochemical redox couple at the air-thin film interface.

differences in microstructural ordering obtained via different deposition techniques may lead to changes in overall charge transport characteristics. This phenomena has been previously observed for (tri)dicyanovinylene-capped oligothiophenes.[65,66] Among all of the present solution-cast devices, compound **10** is found to exhibit the highest mobility ($\mu_e = 0.16$ cm^2/V·s) with an exceptionally high I_{on}/I_{off} ratio (10^7-10^8) and low threshold voltages (0.0−5.0 V) after annealing at 150 °C, indicating that microstructures favorable for efficient charge transport can be achieved by solution casting, likely due to strong long-range intermolecular interactions. Note that this high electron mobility is one of the largest in the literature for a solution-cast n-channel semiconductor film operating in air.[6] Furthermore, the air-stability and an exceptionally high I_{on}/I_{off} ratio makes **10** a very attractive candidate as the n-channel semiconductor in the fabrication of CMOS-like printed organic circuitry. For **10**, the annealing temperature is found to have a significant impact on FET device performance, and a 2 orders of magnitude enhancement in mobility is realized by increasing the annealing temperature from 80 to 150 °C.

Following similar trends as their molecular building blocks, polymers **P3**, **P6**, **P7**, **P8**, **P12**, **P13**, and **P14** are found to exhibit p-channel (**P3**, **P7**, **P12**), ambipolar (**P8**, **P13**, **P14**), and n-channel (**P6**) activity in spin-coated OTFTs. Carbonyl-functionalized bithiophene copolymers **P3**, **P7**, and **P12** exhibit air-stable hole mobilities of 0.001, 3×10^{-4}, and 0.01 cm^2/V·s with I_{on}/I_{off} ratios of $1 \times 10^4-1 \times 10^5$, respectively. Dicyanovinylene-functionalized bithiophene copolymers **P8**, **P13**, and **P14** exhibit highly balanced electron and hole mobilities of 0.5×10^{-4}, 2×10^{-4}, and 2×10^{-4} cm^2/V·s, respectively, with I_{on}/I_{off} ratios of 10^4. Polymer **P8** exhibits ambipolar behavior only under vacuum, whereas polymers **P13** and **P14** are found to operate stably under ambient. To the best of our knowledge, **P13** and **P14** are the first examples of polymeric semiconductors exhibiting both electron and hole mobility under ambient. Dicyanovinylene-functionalized bisindenofluorene homopolymer **P6** exhibits an electron mobility of 0.5×10^{-4} cm^2/V·s with an I_{on}/I_{off} ratio of 10^4 under vacuum.

Discussion

Electrochemical and Optical Properties as a Function of Electronic Structure. To better understand the ionization energetic and mobility properties, the neutral, radical-anion, and radical-cation states of **1**−**12** were evaluated at the B3LYP/6-31G** level of theory; selected geometric parameters (bond lengths and angles) for these states may be found in the Tables S1−S4 of the Supporting Information. For compounds **2** and **7**, good agreement is found between the calculated *gas-phase* and X-ray crystallographic geometries, although the DFT geometries tend to evidence slightly less bond-length alternation (i.e., more delocalization) within the fused carbon−carbon backbones. Calculated electron affinities, ionization potentials, and intermolecular reorganization energies are detailed in Table 5. Across the series, dicyanovinylene functionalization significantly increases the electron affinity. While the magnitude of the impact is lower, dicyanovinylene substitution also renders oxidation more difficult. Thiophene introduction in molecules **3**, **4**, and **7**−**12** has minimal impact on the electron affinity, but (as expected a priori) decreases the ionization potential, thus making oxidation easier. These results, including the relative impact on the ionization energies, are in excellent agreement with the electrochemical reduction and oxidation potentials (Tables 1 and 3).

The impact of dicyanovinylene functionalization on the calculated electronic structures of **1**−**12** is similar (Table 6). For the dicyanovinylene systems, the stronger electron-withdrawing ability of dicyanovinylene versus carbonyl induces considerable energetic stabilization of the LUMO. Contour representations of selected valence molecular orbitals for the model fragments are shown in Figure 16. For both the dicyanovinylene and carbonyl structures, a significant portion of the respective LUMO electron densities are localized on the respective electron acceptor units and at the center of the fused aromatic backbone. Thiophene substitution in **3**, **4**, and **7**−**12** minimally impacts both the LUMO energetics and electron density distribution. The HOMO is also energetically stabilized by dicyanovinylene substitution, although the influence is not as large. The densities of the respective HOMO wave functions are distributed across the fused aromatic backbones with little or no density on the electron-accepting substituents. Unlike the

(65) Chesterfield, R. J.; Newman, C. R.; Pappenfus, T. M.; Ewbank, P. C.; Haukaas, M. H.; Mann, K. R.; Miller, L. L.; Frisbie, C. D. *Adv. Mater.* **2003**, *15*, 1278–1282.
(66) Cai, X.; Burand, M. W.; Newman, C. R.; da Sliva Filho, D. A.; Pappenfus, T. M.; Bader, M. M.; Bredas, J.-L.; Mann, K. R.; Frisbie, C. D. *J. Phys. Chem. B* **2006**, *110*, 14590–14597.

Table 5. Computed Vertical and Adiabatic Electron Affinity (VEA, AEA) and Ionization Potential (VIP, AIP) Energies (eV), Intermolecular Relaxation Energies (λ_1, λ_2), and Total Intermolecular Reorganization Energy (λ_t) As Determined at the B3LYP/6-31G** Level

	reduction					oxidation				
molecule	VEA[a]	AEA[a]	λ_1	λ_2	λ_t	VIP[a]	AIP[a]	λ_1	λ_2	λ_t
1	−1.40	−1.55	0.15	0.15	0.30	7.36	7.24	0.12	0.12	0.24
2	−2.59	−2.76	0.17	0.17	0.34	7.66	7.53	0.20	0.13	0.33
3	−1.62	−1.76	0.14	0.13	0.27	6.63	6.49	0.13	0.14	0.27
4	−2.64	−2.81	0.18	0.16	0.35	6.82	6.67	0.14	0.14	0.29
5	−1.16	−1.25	0.09	0.09	0.17	6.90	6.79	0.11	0.11	0.21
6	−2.17	−2.24	0.06	0.06	0.13	7.15	7.04	0.12	0.11	0.23
7	−1.38	−1.45	0.08	0.08	0.16	6.42	6.31	0.11	0.11	0.22
8	−2.26	−2.32	0.06	0.06	0.13	6.60	6.49	0.11	0.11	0.22
9	−1.62	−1.75	0.14	0.14	0.28	6.71	6.55	0.15	0.15	0.30
10	−2.75	−2.86	0.11	0.11	0.22	6.90	6.74	0.15	0.17	0.32
11	−1.72	−1.84	0.13	0.12	0.26	6.15	6.02	0.11	0.12	0.23
12	−2.79	−2.90	0.11	0.11	0.22	6.25	6.14	0.11	0.11	0.22

[a] Computed using ΔSCF methods. Note that the electron affinities and ionization potentials are calculated by subtracting the total energy on the neutral electronic configuration from the energy of the radical-ion electronic configuration.

Table 6. Selected Molecular Orbital Energies (eV), HOMO−LUMO Gap (eV), Low-Lying Excited-State Energies (eV and nm), Oscillator Strengths, and Excited-State Configurations As Determined at the B3LYP/6-31G** Level

molecule	HOMO−1	HOMO	LUMO	LUMO+1	Δ_{HL}
1	−6.81	−5.97	−2.82	−1.72	3.15
2	−7.00	−6.40	−3.82	−2.94	2.58
3	−6.05	−5.54	−2.87	−1.85	2.66
4	−6.25	−5.78	−3.78	−2.88	2.01
5	−6.64	−5.67	−2.36	−2.20	3.31
6	−6.90	−6.02	−3.27	−3.20	2.75
7	−5.87	−5.43	−2.44	−2.26	2.99
8	−6.04	−5.66	−3.27	−3.20	2.39
9	−6.05	−5.63	−2.90	−1.84	2.72
10	−6.24	−5.88	−3.90	−2.98	1.98
11	−5.42	−5.26	−2.91	−1.88	2.35
12	−5.54	−5.38	−3.87	−2.96	1.51

LUMO, both the energetics and wave function distribution are influenced by the thiophene substitution in **3**, **4**, and **7**−**12**: the HOMO electronic density is fully delocalized across the aromatic core and onto the thiophene units, and the energies are destabilized. The substantial influence of the dicyanovinylene substituents on the LUMO leads to far smaller HOMO−LUMO gaps (Δ_{HL} > 0.4 eV) across the series versus the carbonyl-substituted structures. This is particularly noteworthy for the thiophene-substituted structures, where the additional influence of the thiophenes leads to a substantial decrease in Δ_{HL}. These MO energetic results across the series are in agreement with the experimental estimates of provided by the optical and electrochemical studies (Tables 1 and 3).

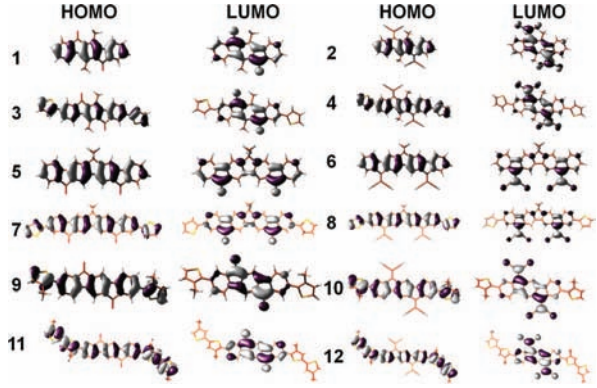

Figure 16. HOMO and LUMO pictorial representation for the present carbonyl- (**1**, **3**, **5**, **7**, **9**, and **11**) and dicyanovinylene-substituted (**2**, **4**, **6**, **8**, **10**, and **12**) semiconductors.

Using the electronic structures of the model compounds, time-dependent DFT (TDDFT) calculations of the lowest-lying excited-state energies are found to track the calculated and experimental Δ_{HL} data closely (detailed information pertaining to low-lying excited-state energies, oscillator strengths, and electronic configurations can be found in Tables S5−S16 of the Supporting Information). The initial transition for each model fragment is characterized as being predominantly HOMO → LUMO in character, with some minor transitions involving other nearby valence MOs. Thus, experimental optical band gaps estimated from the low-energy band edges of the long-wavelength absorption bands should give an accurate estimation of the HOMO−LUMO gap. Additionally, the calculated excited-state energies for the model fragments exhibit red-shifts in the optical absorption maxima with increasing thiophene substitution, as observed experimentally.

Molecular Architecture and HOMO/LUMO Energetics vs FET Performance and Air Stability. The present carbonyl- and dicyanovinylene-functionalized ladder-type molecules and polymers comprise a unique family of semiconductors exhibiting n-channel and/or p-channel charge transport under both vacuum and ambient. Through functional group and core modifications, the intrinsic molecular properties governing majority carrier sign, device performance, and air-stability can be deduced. Analyses of the molecular physicochemical properties, thin film microstructures, and FET device performance/air-stability reveal strong correlations between these parameters.

The relative positions of the HOMO/LUMO energies versus the work function of the source/drain electrodes (Au: 5.1 eV)[25] are crucial in determining the major charge-carrier type in FETs.[67,68] According to a simple Schottky-type charge injection barrier model, the relative electron and hole injection rates have an exponential dependence on the electron (Φ_e) and hole injection barriers (Φ_h), defined as the difference between the metal electrode Fermi level (E_F) and the semiconductor LUMO and HOMO energies, respectively.[68] Furthermore, the relative positions of these orbitals with respect to *H_2O*- and *O_2-oxidation/reduction* reactions determine the ambient stabilities of the electrons/holes during the charge transport process.[11] As shown in Figure 15, the optically/electrochemically estimated HOMO and LUMO energy levels of the present compounds and

(67) Chwang, A. B.; Frisbie, C. D. *J. Phys. Chem. B* **2000**, *104*, 12202–12209.
(68) Facchetti, A.; Mushrush, M.; Yoon, M.-H.; Hutchison, G. R.; Ratner, M. A.; Marks, T. J. *J. Am. Chem. Soc.* **2004**, *126*, 13859–13874.

polymers span a wide range of energies up to 1.1 eV (−3.19 → −4.32 eV for LUMOs and −5.34 → −6.16 eV for HOMOs) providing important information on molecular orbital energetic-majority charge carrier type-ambient stability relationships. In general, decreasing the LUMO energy is found to facilitate electron injection/transport, whereas hole injection/transport is found to be enhanced by increasing the HOMO energy. Thiophene-terminated carbonyl-functionalized compound **7** is a p-channel semiconductor and does not exhibit significant n-channel behavior as a result of a high electron-injection barrier ($\Phi_e = 0.8$ eV). Upon increasing the electron-deficiency of the system (**7** → **3** and **9**), LUMO energies fall and n-channel activities are observed along with p-channel activities as a result of similar electron and hole injection barriers ($\Phi_{e/h} = 0.5-0.6$ eV). In particular, for compound **9**, highly balanced electron and hole mobilities ($\mu_e/\mu_h \approx 1.0$) most likely reflect balanced electron and hole injection barriers. Upon dicyanovinylene functionalization, both HOMO and LUMO energies are lowered even further which results in an increased hole injection barrier and a decreased relative electron injection barrier, thus facilitating electron transport. Experimentally, dicyanovinylene-based compounds **4**, **6**, **8**, and **10** are n-channel semiconductors with negligible p-channel activity, reflecting high hole injection barriers ($\Phi_h = 0.7-0.9$ eV). Similar correlations are also observed for polymeric semiconductors: highly electron-deficient homopolymer **P6** exhibits unipolar n-channel behavior and bithiophene copolymers **P3**, **P7**, and **P12** are found to be p-channel semiconductors. In contrast, donor−acceptor copolymers **P8**, **P13**, and **P14**, having the highly electron-deficient dicyanovinylene (bis)indenofluorene unit as an acceptor and bithiophene as a donor, exhibit ambipolar behavior as a result of the low band gaps (1.3−1.6 eV), resulting in balanced hole/electron injection barriers.

Interestingly, diketone-functionalized compounds **1** and **5** exhibit no FET response for vapor-deposited/solution-cast films, in contrast to their highly reversible electrochemical reduction properties, low LUMO levels (≤ −3.2 eV), and high crystallinities. Such inactivity may be due to minimal orbital overlap in the thin film phase which would reduce the transfer integral for charge transport between molecules in the conduction channel.[26,69] However, the addition of thiophenes to the molecular termini of the core structures (**1** and **5**) facilitates charge transport, yielding ambipolar (**3**) and p-channel (**7**) FET behavior, which indicates the beneficial effects of increased effective π-conjugation length and core size on charge transport.

In general, for the solution-processed OFETs, thin-film crystallinity and grain size are found to be the key parameters in performance, regardless of the intrinsic HOMO/LUMO energetics. Semiconductors forming highly crystalline thin films (judged by XRD peak intensities, the presence of higher order reflections, and rocking curve data) generally have superior FET performance versus films having lower degrees of crystallinity. As an example, although compound **10** forms highly crystalline films with large grains (3−5 μm) due to the favorable orientation of the alkyl chain substituents (β, β') which do not interfere with the molecular planarity and promote self-assembly, thin films of **4** have poor crystallinity with small grains (<0.1 μm) as a result of nonfavorable alkyl chain orientations, disrupting molecular planarity and eventually, intermolecular interactions. Considering the identical molecular backbone structures, the differences in thin-film microstructure and device performance ($\mu_e = 0.0001$ cm^2/V·s for **4** and $\mu_e = 0.16$ cm^2/V·s for **10**) reflect the differences in the DSC- and single-crystal-identified solid-state cohesive forces (vide supra). In addition to the degree of crystallinity, grain size determined by AFM is found to be crucial for efficient charge transport. For **10** and **P13**, although the degree of crystallinity increases significantly on annealing (Figure 10), charge carrier mobility increases only for **10** (0.001 → 0.16 cm^2/V·s) whereas it remains essentially constant (0.0001 cm^2/V·s) for **P13**. AFM analysis shows that the crystallinity increase in **10** is associated with an increase in grain size (0.1 → 5 μm), whereas the grain size remains same (<0.1 μm) for **P13**, suggesting that charge transport here may be largely limited by the grain boundary density since the intermolecular charge hopping across the grain boundaries is not as efficient as the within ordered domains. Here we show that increasing grain size by annealing is a promising approach to enhance the charge carrier mobility, similar to previously reported solution-processed FETs of oligo-/polythiophenes.[70] Generally, we do not observe correlations between device performance and injection barrier; however, the threshold voltage is found to be affected by the magnitude of the injection barrier. For example, when aluminum (work function = 4.2 eV) is used as the source and drain electrodes for thin films of **6** and **P6**, 10−20 V lower threshold voltages are measured compared to the devices with Au electrodes as a result of the lower injection barrier ($\Delta\Phi_e \approx$ 0.9 eV). Compounds **4**, **10**, and **12**, having the lowest LUMO energies (< −4.20 eV) among all compounds examined, exhibit very low threshold voltages of ∼0−5 V, whereas other n-channel compounds (LUMO > −4.0 eV) exhibit higher threshold voltages of ∼20−30 V, probably reflecting, among many factors, the differences in injection barriers which are also evident in the slight curvatures in the source-drain current plots at low source-drain voltages in the output curves of **6** and **8** (Figure 14).

Although the present realization of thermodynamically air-stable n-channel semiconductors shows that low LUMO energies are necessary for efficient charge transport in ambient, the exact parameters governing the air-stability still remain incompletely resolved.[7] Therefore, it is still important to further understand the structural and electronic criteria leading to the ambient stability in n-channel organic semiconductors. To investigate the effects of molecular energetics on device ambient stability, HOMO/LUMO energies were finely tuned ($\Delta \approx 0.1$ eV) over 1.1 eV for a series of semiconductors, and their impact on the ambient stability explored (Figure 17). FETs fabricated with **4**, **10**, **12**, **P13**, and **P14** operate stably in air, without any device performance degradation, whereas the other n-channel semiconductors **3**, **6**, **8**, **9**, **P6**, and **P8** only operate satisfactorily under vacuum. Assuming similar thin film microstructures and morphologies for the present molecules/polymers, and assuming that Marcus reorganization energies, intermolecular orbital overlap, interface dipoles, and charge traps are essentially constant due to molecular structure/device similarities, the differences in air-stability must mainly be a function of LUMO energy.[13] The low LUMO energies of the former semiconductors can stabilize the injected charge carriers against the reactions with ambient species (O_2/H_2O). Detailed analysis of the molecular/polymeric orbital energetics indicates that an onset

(69) Kim, E.-G.; Coropceanu, V.; Gruhn, N. E.; Sanchez-Carrera, R. S.; Snoeberger, R.; Matzger, A. J.; Bredas, J.-L. *J. Am. Chem. Soc.* **2007**, *129*, 13072–13081.

(70) Mcculloch, I.; Heeney, M.; Bailey, C.; Genevicius, K.; Macdonald, I.; Shkunov, M.; Sparrowe, D.; Tierney, S.; Wagner, R.; Zhang, W. M.; Chabinyc, M. L.; Kline, R. J.; McGehee, M. D.; Toney, M. F. *Nat. Mater.* **2006**, *5*, 328–333.

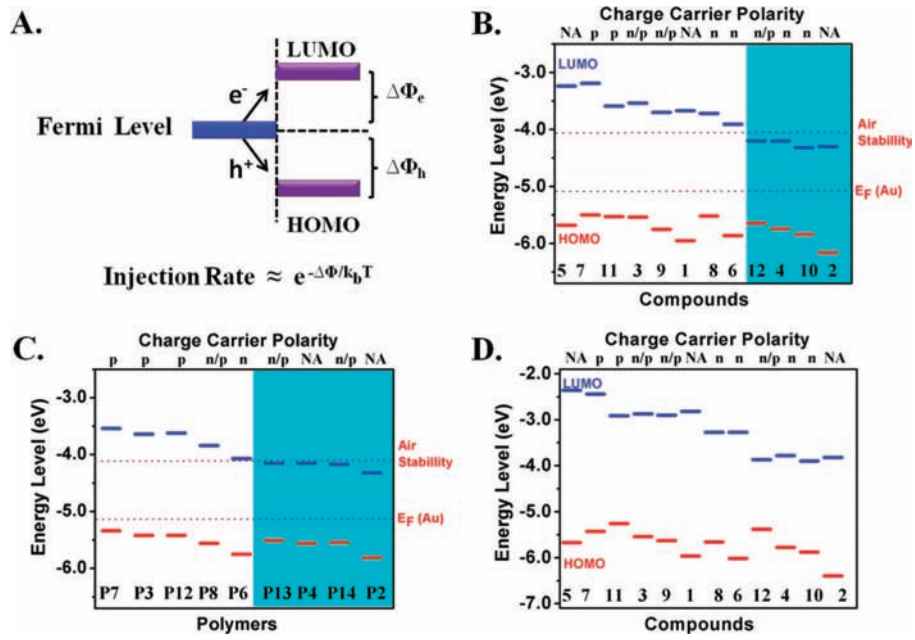

Figure 17. (A) Schematic of a Schottky-type injection barrier between a metal electrode and an organic semiconductor, showing electron/hole injection barriers. The energy diagram for compounds **1**−**12** and polymers **P2**, **P3**, **P6**, **P7**, **P8**, and **P12**−**P14**, showing experimentally estimated (B and C) and theoretical (D) HOMO/LUMO energy levels, and charge carrier polarity. The blue region indicates TFT devices with ambient stability. The dashed lines indicate the Fermi level of the gold electrode and the air-stability limit.

LUMO energy of −4.1 to −4.0 eV is essential to stabilize electrons during charge transport, and an overpotential of 0.9−1.0 eV is operative in the reactions of negatively charged organic π-anions with O_2/H_2O. This overpotential must reflect the energetic barriers to the penetration of ambient species into the active conduction channel,[1,5,62] which is in proximity to the gate dielectric and ∼40−50 nm underneath the semiconductor/air interface.[71] The density of grain boundaries, through which ambient species most likely penetrate the film, doubtless affects the magnitude of the overpotential. We suggest that the differences between the actual energies of the film electrons during charge transport on OTS-treated Si/SiO_2 substrates and the LUMOs estimated from solution/thin-film cyclic voltammetries also contribute to the exact overpotential value.

Although the thin-film microstructure is crucial to FET device performance, its impact on ambient stability is still unresolved. If the semiconductor film microstructure (morphology and crystallinity) plays a role in ambient stability, one would expect a thin film with a high degree of crystallinity, large grains, and a low density of grain boundaries to be less susceptible to the diffusion of environmental traps into the thin film, and therefore to be more stable in air compared to a film with a high density of grain boundaries and a low degree of crystallinity. We investigated the air stability trends in solution-cast thin films of compound **10**. The unique thermal response of the TFT devices based on **10** allows us to prepare thin films with a wide range of grain sizes (0.1−5 μm) with morphologies changing from small ball-like grains to large plate-like grains, and having a wide range of crystallinities, including different crystalline phases, XRD intensities (200−60 000 counts/s), and FWHMs (0.2−0.4°). As shown in Figure 11, regardless of these microstructural variations, all **10** thin films exhibit similar stability trends in air with little to no degradation. In marked contrast, for the films of semiconductors with LUMOs outside the ambient stability window (> −4.0 to −4.1 eV), regardless of film microstructure, devices always exhibit severe degradation in air. These observations argue that although film microstructure is important for the device performance, its contribution to the air-stability is minimal, and ambient stability is mainly governed by LUMO energetics, consistent with other recent work on core-cyanated perylenes.[7] These results are critical to the development of new air-stable n-channel semiconductors.

Conclusions

A new family of carbonyl-/dicyanovinylene-functionalized bis(indenofluorene) compounds **1**−**12** and their corresponding homo- and copolymers **P1**−**P14** has been synthesized and characterized by DSC, TGA, melting point, solution/thin-film UV−vis, PL, and cyclic voltammetry measurements. Optical and electrochemical data demonstrate that HOMO/LUMO energetics can be finely tuned in steps of ∼0.1 eV over a window of 1.1 eV via core and functional group modifications. Vapor-deposited and solution-cast thin films are characterized by XRD and AFM, indicating the presence of well-organized lamellar microstructures with the common preferential molecular/chain "edge-on" orientation relative to the substrate. Strong correlations are seen between molecular physicochemical properties, thin film microstructures, and FET device performance/air-stability. We observe that the relative positions of HOMO and LUMO energies versus the source and drain electrode work functions affect the charge injection barriers, which eventually determine the charge carrier characteristics. For the semiconductors with large electron injection barriers and low hole injection barriers (**7**, **11**, **P3**, **P7**, and **P12**), p-channel (μ_h up to 0.01 $cm^2/V\cdot s$) behavior is observed. For the semiconductors with balanced electron and hole injection barriers (**3**, **9**, **12**, **P8**, **P13**, and **P14**), ambipolar (μ_e up to 0.01 $cm^2/V\cdot s$ and μ_h up to 0.006 $cm^2/V\cdot s$) behavior is observed, including the first examples of molecular and polymeric ambipolar semiconductors operating in air, achieved via the synthesis of low band gap (1.36−1.40 eV) donor−acceptor structures. Furthermore, n-channel behavior

(71) Hamerin, W. J.; Wood, R. E. In *Handbook of Physics*; Condon, E. U., Odishaw, E. U., Eds.; McGraw-Hill: New York, 1958.

(μ_e up to 0.02 $cm^2/V \cdot s$) is observed for semiconductors **4**, **6**, **8**, **10**, and **P6** with low electron injection barriers. For semiconductors with sufficiently low LUMO energies (< −4.1 eV), air-stable *n*-channel behavior with mobilities up to 0.16 $cm^2/V \cdot s$ are realized with exceptionally high on/off ratios of 10^7-10^8, exhibiting some of the best solution-based FET performance reported to date for an n-channel semiconductor in ambient. Analysis of the air-stability of a series of thin semiconductor films with different crystallinities, orientations, and morphologies reveals that air-stability for the present semiconductors is principally governed by the LUMO energy with negligible contribution from film microstructure. We estimate the onset LUMO energy for electron stabilization during charge transport to be −4.0 to −4.1 eV, indicating an overpotential of 0.9−1.0 eV to the reaction of the n-type charge carriers with O_2/H_2O. Density functional theory (DFT) calculations fully explain the observed electronic structure trends associated with core structure and functional group alterations. The findings presented here demonstrate that through rational molecular/macromolecular design guided by computational modeling, a new family of highly electron-deficient ladder-type semiconductors is realized with desired molecular/OFET properties. Furthermore, the present results provide key information related to the structural and electronic criteria controlling the air-stability of n-channel materials.

Acknowledgment. We thank ONR (N00014-05-1-0766), AFOSR (FA9550-08-1-0331), and Polyera Corporation for support of this research, and the NSF-MRSEC program through the Northwestern University Materials Research Science and Engineering Center (DMR-0520513) for providing both support and characterization facilities. We thank Dr. E. Szuromi and Prof. R. F. Jordan for hospitality with GPC measurements.

Supporting Information Available: Synthetic procedures for characterizations of compounds **1**−**12**, monomers **M1**−**M6**, and polymers **P1**−**P14**; representative OFET plots of devices fabricated with polymer **P13** and **P14**; AFM images of the thin films of **3, 6**, **11**, and **P13**; single-crystal structure data for compounds **7**, **M2**, and **M4**. This material is available free of charge via the Internet at http://pubs.acs.org.

JA809555C